Environmental Earth Sciences (2021) 80:457
https://doi.org/10.1007/s12665-021-09741-0

ORIGINAL ARTICLE

Development of the coseismic landslide susceptibility map of the island of Lefkada, Greece

Aglaia Matsakou[1] · George Papathanassiou[2] · Vassilis Marinos[3] · Athanasios Ganas[4] · Sotirios Valkaniotis[2]

Received: 5 October 2020 / Accepted: 9 June 2021 / Published online: 24 June 2021

Abstract

The island of Lefkada, Greece periodically suffered environmental and structural damages induced by earthquakes. During the twenty-first century, two moderate events of magnitude M > 6 occurred in 2003 and 2015 (M6.2 and M6.5, respectively). The dominant type of the earthquake-induced environmental failures was rock falls and slides that were widespread at the western part of the island. The goal of this study is to assess the earthquake-induced landslide susceptibility in the island of Lefkada and to compile a relevant susceptibility map. To achieve this, we took into account the inventories of coseismic slope failures, that were compiled for the 2003 and 2015 events. The spatial distribution of landslides in relation to the causal factors of geology and topography-oriented parameters were statistically analyzed based on the landslide susceptibility index LSI and the Likelihood ratio LR methods. In order to be able to validate the developed map, the dataset of slope failures was separated into two groups: training set (inventory of 2015 event) and testing one (inventory of 2003 earthquake). The outcome arisen by these analyses is that the geological formation of limestones of Paxos zone and the northwest-facing slopes are considered as the most causal factors for the triggering of slope failures. Considering the factor of slope angle, the LSI-based method shows that the highest frequency of slope failures is related to slope angles between 40° and 50° while the LR approach indicates the areas of high-angle slopes (60°–80°) as the most susceptible one. Taking into consideration that the susceptibility map is compiled based on the spatial distribution of coseismic slope failures triggered by earthquakes occurred both on the northern (2003 event) and southern part (2015 event) of the Lefkada segment of the Cephalonia Transform Fault (CTF), it can be characterized as a complete susceptibility map. Therefore, it is believed that can be used by public agencies and civil protection authorities since the locations of the slope failures triggered by future earthquakes are shown and consequently the elements of the manmade environment, e.g. road network that will be disrupted due to coseismic slope failures could be forecasted.

Keywords Coseismic landslides · Lefkada · Landslide susceptibility index · Likelihood ratio

Introduction

Earthquakes often trigger numerous landslides (e.g. Keefer 1984; Rodriguez et al. 1999; Marzorati et al. 2002; Sassa 2005), which may severely affect the manmade environment. Experience has shown that seismically induced landslides represent one of the most damaging hazards associated with earthquakes in countries with high seismicity (Ayalew et al. 2011). According to Jibson et al. (2000) the effect of seismically-induced landslides on human lives and facilities may exceed in some cases the damage directly connected to the generated strong ground motion.

Recently, Marano et al. (2009) showed that 5% of fatalities related to earthquakes were caused by landsliding and that they were the third largest contributor to fatalities

✉ George Papathanassiou
gpapatha@civil.duth.gr

1 Laboratory of Engineering Geology and Hydrogeology, Faculty of Sciences, School of Geology, Aristotle University of Thessaloniki, 54124 Thessaloníki, Greece

2 Department of Civil Engineering, Polytechnic School, Democritus University of Thrace, 67100 Xanthi, Greece

3 Geotechnical Department, School of Civil Engineering, National Technical University of Athens (NTUA), 9, Iroon Polytechniou Street, 15780 Athens, Greece

4 Institute of Geodynamics, National Observatory of Athens, Lofos Nymfon, Thission, 11810 Athens, Greece

after building collapse and tsunamis (Jessee et al. 2018). Moreover, coseismic landslides have also been shown to be a major cause of disruption to lifelines, mainly in mountainous regions, impeding emergency response efforts (Bird and Bommer 2004; Jessee et al. 2018). As a consequence, the earthquake-induced damages to lifelines, e.g. roads and transportation lifelines, cause delays of rescue efforts (Jessee et al. 2018). According to early estimates of the damages caused by the Kaikōura, New Zealand 2018 earthquake, the possible cost of repair and rebuilding work was at about $2bn (Kiernan 2016), while a permanent loss of through traffic for Kaikōura severely undermine the sustainability of the town and its tourism sector. Similar consequences have been reported in Greece and particularly at the islands of Lefkada and Cephalonia where the earthquakes of 2003, 2014 and 2015, respectively induced extensive damages to infrastructure networks. In particular, the main coastal road at the island of Lefkada was severely damaged by landslides triggered both by the 2003 and 2015 events, leading to the closure of the road network. Consequently, the local economy, which is mainly based on the tourism sector, was strongly affected.

The last 20 years numerous studies have been performed aiming to examine the spatial distribution of the earthquake-induced landslides and to assess the coseismic landslide susceptibility of the affected by the event area. Chigira and Yagi (2006), Imanishi et al. (2006), Hikima and Koketsu (2005) and Sidle et al. (2011) focused on the 2004 Mid Niigta earthquake in Japan, while Huiming et al. (2010), Yin et al. (2009), Xu et al. (2009) and Cui et al. (2009) reported the slope failures triggered by the Great Wenchuan Earthquake in China. Considering the Kaikōura Earthquake, New Zealand, Massey et al. (2020) and Dellow et al. (2017) reported the generated failures, while Stringer et al. (2017) presented the geotechnical aspects of this event.

The assessment of the landslide susceptibility is the first step towards the evaluation of landslide hazard and is defined as the likelihood of a landslide occurring in an area in relation to the local geomorphological conditions (Brabb 1984). The assessment of susceptibility can be achieved by taking into consideration the regional landslide predictive models that estimate "where" landslides are likely to occur over a given region based on a set of geoenvironmental characteristics (Guzzetti et al. 1999). The techniques that have been developed and widely used for the assessment of susceptibility can be mainly subdivided into direct and indirect methods. Considering the former approach, a geoscientist, i.e. geomorphologist, can directly determine the level of susceptibility based on his/her experience and information related to terrain conditions, whereas the indirect mapping statistical models are used to forecast likely to landslide areas, based on the information obtained from the interrelation between the spatial distribution of landslide conditioning factors and the landslide zones (Papathanassiou et al. 2013).

Nowadays, earth scientists mainly use geographic information system (i.e. GIS based) techniques and remote sensing data for compiling landslide susceptibility and hazard maps and for evaluating the relevant risk within an area. More specifically, these GIS-based techniques are considered as very suitable for indirect landslide susceptibility mapping, in which all possible landslide-contributing terrain factors are entered into GIS environment and combined with the spatial distribution of coseismic slope failures, i.e. landslide inventory map (Bonham-Carter 1994; Chung et al.1995; van Westen et al. 2003; Papathanassiou et al. 2013).

The widely used methods for the assessment of landslide susceptibility are: Landslide Susceptibility Index (LSI), (Dai and Lee 2002; Ercanoglu and Gokceoglu 2004; Lee 2007; Pradhan and Youssef 2010; Papathanassiou et al. 2013; Chalkias et al. 2014; Kavoura and Sabatakakis 2019; Rui-Xuan et al. 2020), Logistic Regression (LoR), (Duman et al. 2006; Nandi and Shakoor 2010; Schicker and Moon 2012; Schlögel et al. 2017; Lombardo and Mai 2018; Wei et al. 2019), Likelihood Ratio (LR), (Lee 2004; Kanungo et al. 2011; Sharma et al. 2014), and Discriminant Analysis (DA), (Baeza et al. 2010; He et al. 2012).

Nowadays, these methods are being used in combination with innovative methods, such as Artificial Neural Networks (ANN), Support Vector Machines (SVM), hybrid integration of MultiBoosting based on the two artificial intelligence methods (the radial basis function network (RBFN) and Credal Decision Tree (CDT) models). More specifically, Zhao et al. (2020) applied the LR, ANN, and SVM models in order to generate landslide susceptibility maps based on the developed earthquake-induced landslide inventories of 2004 Mid-Niigata event. The developed ROC curve clearly demonstrated that the map obtained from the ANN model performed the best among the three models. Moreover, Guirong et al. (2020) proposed that the large-scale landslide susceptibility prediction can be utilized to devise strategies for infrastructural and detailed land use planning. They concluded that the most positive impact classes exist at low slope angles and high values of SPI (Stream Power Index), STI (Sediment Transport Index), and TWI (Topographic Wetness Index). Dou et al. (2019) compared the abilities of the statistical Probabilistic Likelihood-Frequency Ratio (PLFR) model, Information Value (InV) method, Certainty Factors (CF), Artificial Neural Network (ANN), and ensemble Support Vector Machine (SVM) for the landslide susceptibility mapping using high-resolution-light detection and ranging digital elevation model.

This study aims to develop an earthquake-induce landslide susceptibility map of the island of Lefkada by taking into consideration the information provided by the recently

developed inventories of 2003 and 2015 earthquakes. It should be pointed out that the outcome of this study can be considered as a complete susceptibility map since for its development we used updated data triggered by the activation of both segments of the Cephalonia Transform Fault (CTF). This fault is located offshore the western coast of the island and is considered as the main and most hazardous seismogenic source in the area. More specifically, the two landslide inventories (Papathanassiou et al. 2017b, 2021) that were used for the development of the susceptibility map have been compiled based on the data provided by earthquakes occurred on the northern part (14/8/2003) and on the southern part (17/11/2015 event) of the island. The inventory of the 2015 earthquake was used as the training dataset, while the data provided for the penultimate event (2003) are used for the validation of the developed susceptibility maps.

Geology and tectonic setting

The geology of the Lefkada island was studied in detail by Bornovas (1964) and Cushing (1985). Lefkada's geological formations are sedimentary rocks (mostly carbonates) that belong to the Ionian and Paxos (Pre-Apulian) zones of the External Hellenides (Fig. 1a; Bornovas 1964; B.P. Co ltd 1971; Cushing 1985; Underhill 1988). The boundary between the two different geological zones—Ionian and Paxos, runs in an approximate NW–SE direction through this region and outcrops onshore south-central Lefkada Island near Hortata village, in the form of a buried thrust fault (Ionian Thrust) covered by scree and late Quaternary deposits. The majority of Paxos and Ionian formations comprise limestones, dolomites and Paleogene—Miocene marls and carbonates. Small isolated outcrops of evaporates can be found inside the Ionian formations. Pleistocene and Holocene coastal deposits are extended in the northern edge of Lefkada, in the plain of Vassiliki and in the coastal plain of Nydri. A Pleistocene terrestrial series of sediments is found along the elongated Dragano Valley, while red beds and terrestrial deposits are also found in individual karst depressions around the island. Large Holocene scree and debris cones are found along the western coast of Lefkada and the slopes of the northern Vassiliki valley (Bornovas 1964; Cushing 1985). Figure 1a shows the distribution of the main geological formations based on the map by Cushing (1985).

The island of Lefkada is part of the high seismicity Ionian Sea area. This is due to the complex crustal deformation resulting from the subduction of the African plate towards NE and the Apulian platform continental collision (Hatzfeld et al. 1995; Clement et al. 2000; Ganas et al. 2013). The main active tectonic structure, accommodating the relative motion of these lithospheric plates, is the dextral strike-slip Cephalonia–Lefkada Transform fault (CTF; Scordilis et al. 1985; Louvari et al. 1999; Sachpazi et al. 2000). This 140-km long CTF fault zone has a GPS slip-rate bracketed between 10 and 25 mm/yr (Pérouse et al. 2012) accommodating a strain rate of 225 ± 20 ns/yr (Caporali et al. 2016).

The main bedrock structures are NW–SE thrust faults, imbricating the Ionian limestone over Miocene marls of Paxos zone of the Hellenides (Bornovas 1964) from NE towards SW and a system of neotectonics faults. The NE–SW to NNE–SSW trending neotectonic main faults are normal faults with a significant right-lateral component, while some minor faults NW–SE trending show left-lateral character (Cushing 1985; Pavlides et al. 2004; Rondoyanni et al. 2007). Taking into consideration, the morphology and the fresh escarpments, most of them can be considered as active or possibly active minor structures. Along the west coast, steep morphology is due to the offshore CTF and its onshore sub-parallel fault, i.e. the Athani-Dragano fault (Cushing 1985; Rondoyanni et al. 2007, 2012; Papathanassiou et al. 2017a). Athani-Dragano fault is an NNE–SSW-striking oblique fault forming an elongated continental basin, creating a characteristic relief and marked on satellite images and aerial photos. Exposed striated fault planes can be observed along the fault trace. The Athani-Dragano fault seems to terminate to the north near Komilio village, forming a series of splay (normal) faults, striking NE–SW, and its southern continuation is today eroded and presumed to be offshore to the west of the coast. The fault zone was active from Late Pliocene to possibly Middle-Late Pleistocene (Cushing 1985), but field examination shows no clear evidence of a recent (Latest Pleistocene–Holocene) re-activation (Papathanassiou et al. 2017a). The recent (Holocene) activity and seismic behavior of the other neotectonic faults are unknown (Rondoyanni et al. 2007).

Earthquake-induced landslides in the island of Lefkada

The island of Lefkada is considered as one of the most active tectonic areas in Europe and one of the most active zones in the eastern Mediterranean region (Ganas et al. 2016). According to Papathanassiou et al. (2005), more than 25 earthquakes occurred from 1612 until today, which sometimes appears in couples (twin or cluster events) with period of occurrence ranging between 2 months and 5 years.

Many researchers have performed studies from different perspectives and for different research purposes in the island of Lefkada. Papathanassiou et al. (2013) developed the first landslide inventory map of the 2003 earthquake, integrating satellite imagery, and reports from field surveys. Ganas et al. (2016) tested the relocation of seismicity and inversion of geophysical (GPS, InSAR) data, measuring the coseismic deformation by continuous GPS stations of NOANET (the

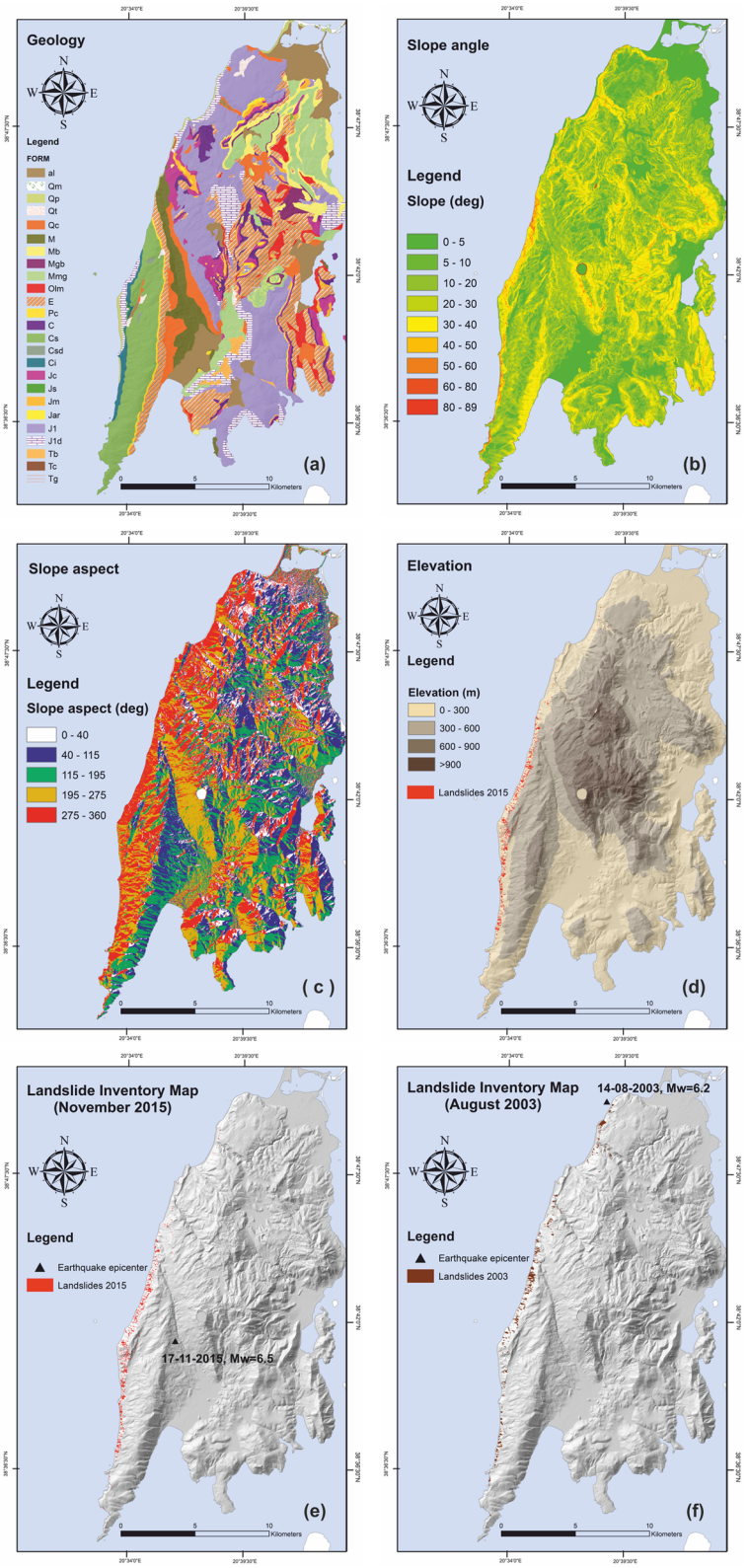

Fig. 1 **a** Geological map of Lefkada island (based on the Cushing 1985), where al, Qm, Qp, Qc: Pleistocene and Holocene alluvial and coastal deposits, Qt: Pleistocene travertine, M: Miocene marl, Mb: Miocene Breccia or Conglomerate, Mgb, Mmg: Miocene sandstones, Olm: Miocene flysch, E: Eocene limestones, Pc: Paleocene limestones, C,Cs, Jc, Js, Ci: Cretaceous limestones, Csd: Cretaceous Dolomitic limestone, Jm: Jurassic limestone, Jar: Ammonitico Rosso facies, J1: limestone of Pantokratora, J1d: Dolomite, Tb: Triassic Breccia with limestone and dolomite, Tc: Triassic Dolomitic limestone, Tg: evaporites, **b** Slope angle map of the Lefkada island, **c** Slope aspect map of the Lefkada island, **d** Elevation map of the Lefkada island, **e** Landslide inventory map of the 2015 event, (data from Papathanassiou et al. 2021), and **f** Landslide inventory map of the 2003 event, (data from Papathanassiou et al. 2017b)

NOA GPA network) and by InSAR, and producing a coseismic uniform-slip model from inversion of InSAR data and permanent GPS stations. According to Ganas et al. (2016), the 2003–2015 pattern of seismicity in the Ionian region indicates the existence of a 15-km seismic gap offshore NW Cephalonia.

Furthermore, Kazantzidou-Firtinidou et al. (2016) assessed the macroseismic intensity of 2015 event as VIII, based on the reported damages and the vulnerability per building typology. In addition, they presented the distribution of the damage per building category, based on the site surveys and post-seismic usability characterization by the local Earthquake Rehabilitation Organization. Lekkas et al. (2016) reported the Earthquake Environmental Effects (EEE) and damages to buildings and infrastructure induced by the 2015 event. Ilieva et al. (2016) took into account seven ascending ENVISAT/ASAR images, in order to process six co-seismic interferograms and by the inversion of the data from the observed fringes, a model of the activated fault was calculated; the inferred fault is a pure dextral strike-slip fault, dipping $59^{o} \pm 5^{o}$ eastward, 16 ± 2 km long and 10 ± 2 km wide.

Papathanassiou et al. (2017a) present in a quantitative way the coseismic failures generated by the 2015 earthquake, as well as the assessment of the macroseismic intensity based on the ESI-07 scale; the maximum intensity, assigned as VIII up to IX, was identified at the coastal area of Egremnoi. They highlighted that this event triggered environmental effects mainly at the western part of the island, while the severity of the earthquake-induced failures decreased moving towards the eastern part. Furthermore, Tsangaratos et al. (2018) compiled a landslide susceptibility map of the island of Lefkada, by applying a novel expert-based approach.

Considering the generated seismic ground motion, Papaioannou et al. (2018) pointed out that the peak horizontal acceleration was recorded as 0.24 g at Ag. Nikitas (epicentral distance 14 km) and 0.41 g at Chortata (4 km epicentral distance). Grendas et al. (2018) presented the results of an engineering geological mapping of earthquake-induced landslides in the southern part of Lefkada that took place in a zone where high severity slope failures were triggered, at Egremnoi and Gialos areas. Applying the Newmark's (1965) approach, they concluded that the generated by the earthquake peak ground acceleration at these areas should have been at least 0.45 g, to trigger these types of slope failures. This outcome is in agreement with the recorded value of the strong ground motion in the area, as it was presented by Papaioannou et al. (2018).

Summarizing, it is pointed out that the slope failures triggered by the 2003 and 2015 earthquakes were mainly reported on the western part of the island. Most of the failures triggered by the penultimate event were classified as rockfalls and slides and reported on the north-western part, while small size scattering phenomena were also reported on the central part (Papathanassiou et al. 2005).

Similar earthquake-related phenomena, e.g. rockfalls, rock slides, landslides, and road-fill failures were triggered by the 2015 earthquake (Papathanassiou et al. 2017a, 2021; Zekkos et al. 2017; Saroglou et al. 2018). The areas that were widely affected by these phenomena are located in the south-western part of the island. Regarding the eastern part of the island, the earthquake triggered only sparse and small size rock falls and rock slides on road cuts. Nowadays, most of the damages on the road network, caused by the coseismic landslides have been restored as it can be seen in the following figures (Fig. 2).

Assessment of the coseismic landslide susceptibility at the island of Lefkada

As it has been highlighted in preceding sections, the goal of this study is to assess the coseismic landslide susceptibility at the island of Lefkada and to develop a relevant map. In order to achieve this, two statistical methods were applied; the statistical methods of Landslide Susceptibility Index (LSI), developed by van Westen (1997) and the Likelihood Ratio (LR). In LSI, each causal factor map is combined with the landslide distribution map, and weighting values based on the landslide densities are calculated for each parameter class (Soeters and van Westen 1996). More specifically, a weight-value for a parameter class or unit is defined as the natural logarithm of the landslide density *i,* the class divided by the landslide density in the entire map. The natural logarithm is used to give negative weights when the landslide density is lower than normal and positive when it is higher than normal (van Westen 1997).

This method is based on the following formula:

$$W_i = \ln \frac{\text{denClass}}{\text{denMap}} = \ln \left(\frac{\frac{N_{\text{pix}}(S_i)}{N_{\text{pix}}(N_i)}}{\frac{\sum N_{\text{pix}}(S_i)}{\sum N_{\text{pix}}(N_i)}} \right) \quad (1)$$

Where W_i = the weight given to a certain parameter class (e.g. a rock type or a slope class); densClass = the landslide density within the parameter class; densMap = the landslide density within the entire map; $N_{\text{pix}}(S_i)$ = number of pixels, which contain landslides, in a certain parameter class; $N_{\text{pix}}(N_i)$ = total number of pixels in a certain parameter class.

The LR approach can be applied for the determination of the observed relationship between the causative factors and landslide occurrences (Kanungo et al. 2011), and is computed as the ratio of the percentage of the landslide pixels L_i to the percentage of the non-landslide pixels N_i (Eq. 2). In particular, the LR is estimated for every class

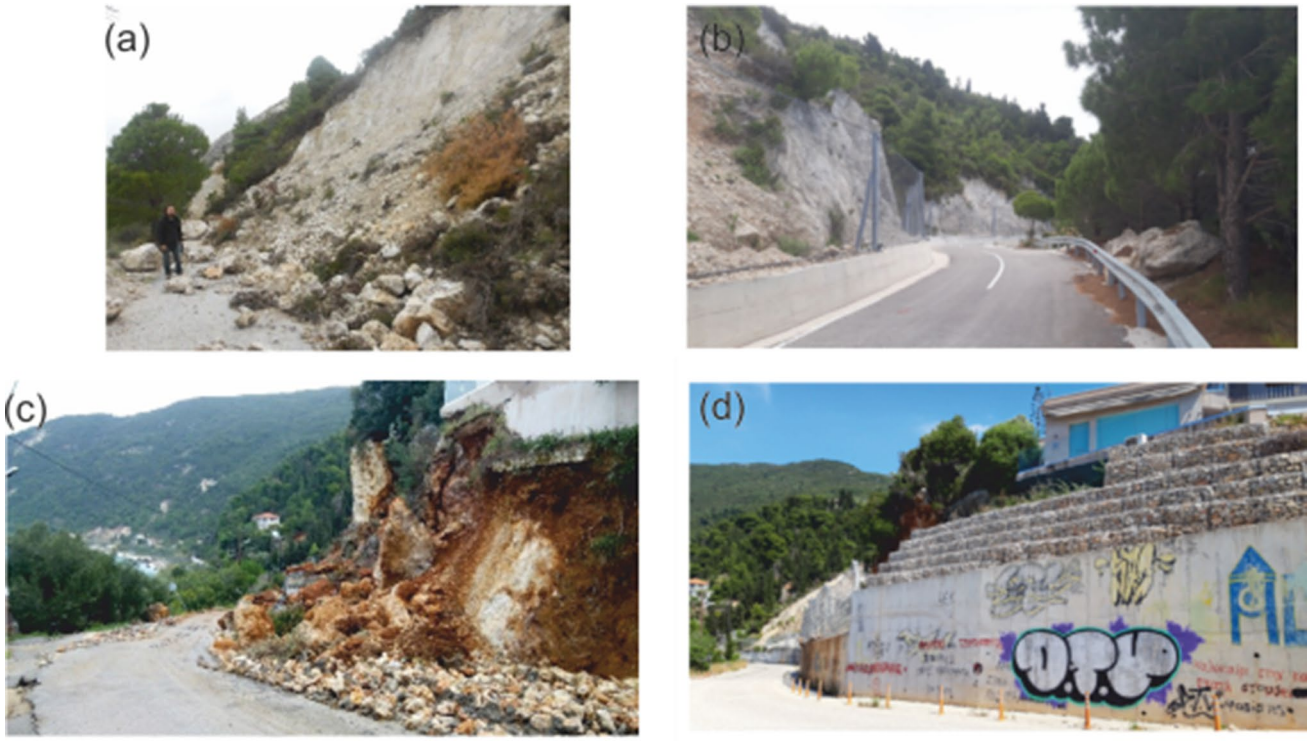

Fig. 2 Comparative pictures showing: **a** Rock slide at the area of Gialos (photo taken on November 21th, 2015), **b** rockfall protection mesh at the same area (photo taken on May 26th, 2020), **c** rockfalls in the entrance of the village of Agios Nikitas (photo taken on November 19th, 2015), **d** Construction of retaining wall (gabions, concrete wall) at the same area (photo taken on May 26th, 2020)

per factor, i.e. geology, slope angle, slope aspect and elevation. For higher values of LR, the impact of the specific factor to the landslide occurrence is high, while for LR < 1 is low (Lee 2004). Afterwards, the computed likelihood ratios of each factor per pixel are summed in order to calculate the total susceptibility index (SI) per pixel. According to Lee (2004), a higher susceptibility is related to high values of SI and vice versa, a lower value means lower susceptibility and more stability. The total computed index should be normalized, classified and grouped into three or five classes for visual interpretation.

$$\mathrm{LR}_i = \frac{L_i}{N_i} \tag{2}$$

where

$$L_i = \frac{I_i \times 100}{P} \tag{3}$$

and

$$N_i = \frac{M_i \times 100}{\mathrm{NP}} \tag{4}$$

L_i is the total number of pixels with landslides in the area covered by the class of factor and P is the total number of pixels with landslides in the study area. Similarly, M_i is the total number of pixels without landslides in the area covered by the class of factor and NP is the total number of pixels without landslides in the study area (Sharma et al. 2014).

To be able to perform these statistical approaches, the vector data provided by the landslide inventory of 2015 event (Papathanassiou et al. 2021) and by the geological map (Fig. 1a) were initially converted into raster data (cell size 10 × 10 m). Similar procedure was followed for the products derived from the digital elevation model DEM (5 m resolution) of Lefkada [i.e. slope angle, slope aspect and elevation map (Fig. 1b, c, d)]. Afterwards, the spatial distribution of landslides was statistically analyzed in relation to the factors of geology and topography, to investigate their influence in landsliding phenomena. Subsequently, all these factors were overlaid as thematic layers and the resulted maps were classified at 5 susceptibility classes for the Landslide Susceptibility Index and Likelihood ratio methods, respectively. Both developed susceptibility models were further analyzed by calculating frequency values to estimate the success rate, based on the information provided by the landslide inventory of 2015

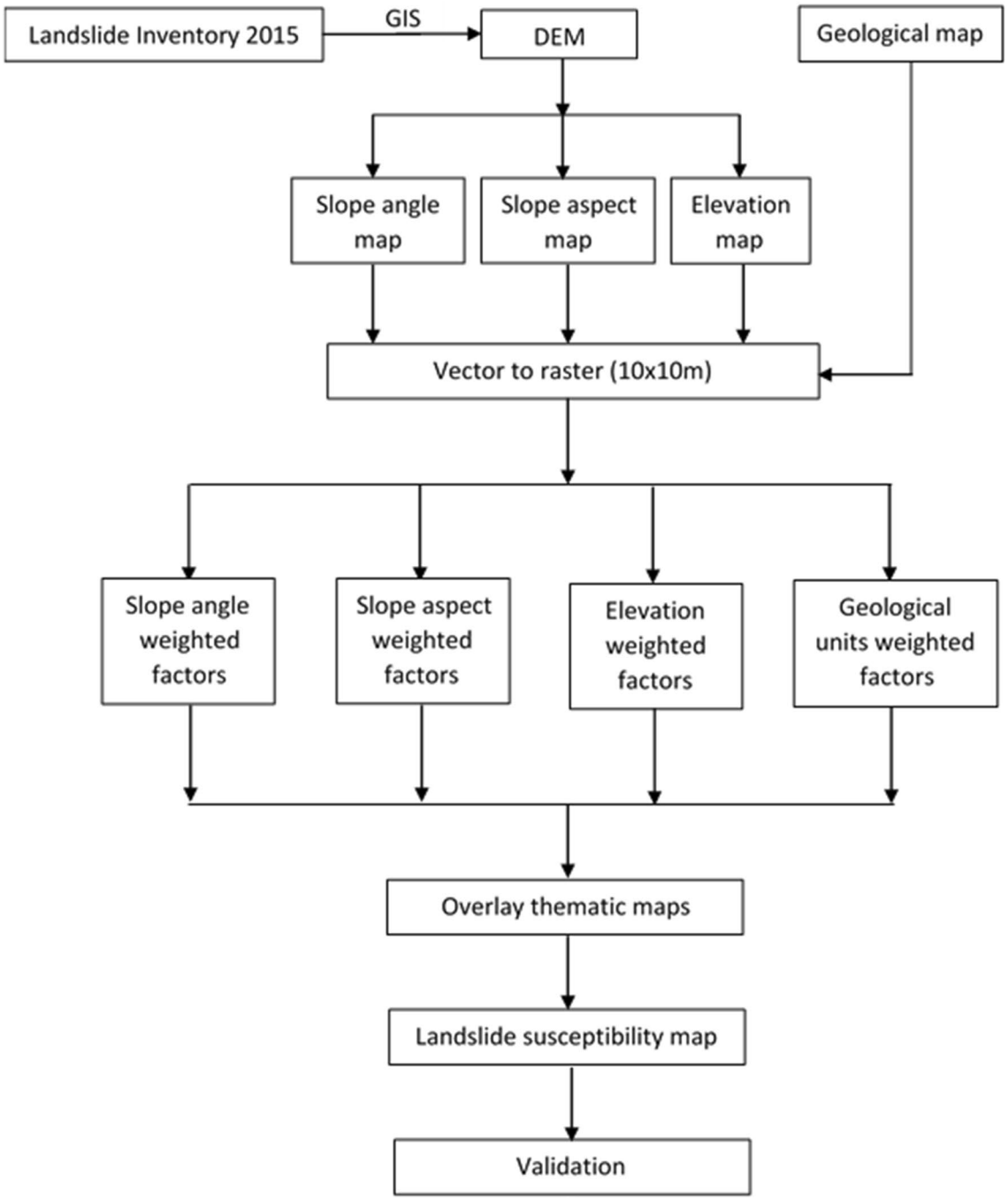

Fig. 3 Flow chart of landslide susceptibility analyses (LSI and LR) conducted in this study

earthquake (Fig. 1e). The validation of these maps was realized by statistically comparing them with the inventory of 2003 earthquake (Fig. 1f) (Papathanassiou et al. 2017b). In this way, the success and prediction rate curves per model were plotted for examining the performance of our models. In Fig. 3, is shown the flow chart of landslide susceptibility analyses conducted in this study. It must be mentioned that, on both inventories, the source and runout area were not mapped separately, and that the surface of the study area is 301.98 km^2. The percentage of the area affected by landslides is 0.43% (1.29 km^2) and 0.57% (1.71 km^2) based on the inventory of 2015 and the 2003 event, respectively (Fig. 1e, f).

Landslide susceptibility index method

In this section is presented the outcome arisen by the application of the LSI methodology to the island of Lefkada.

Landslide density

Initially, the spatial distribution of the seismically-induced landslides of the 2015 earthquake was correlated with each of geological and topographical factors in order to develop relevant landslide density maps. The density is expressed as the percentage of the area affected by landslide activity. Following the definitions proposed by Ayalew et al. (2011) for computing the frequency of landslide activity, we adopted that the unit landslide density is the ratio between areas affected and not affected by landslides in each geological unit, and the total landslide density is the area affected by landslides in each geological unit divided by the total study area, determining the susceptibility of geological units for failure. Similarly, statistical analyses were also performed for the other three factors, slope angle, slope aspect and elevation that were taken into account in this study.

Considering the correlation of the spatial distribution of landslides with the geological units, most of the landslides are reported in areas covered by limestone (~65%) (Table 1). In particular, the highest concentration of landslide activity per geological unit shows the group of units Ci-Cs-Csd (2.18%), where although the fact that covers only 9.97% of the study area, the landslide activity is almost 51.21% of the whole landslide activity in the island. It is followed by the unit of J1-J1d that covers the 28.34% of the study area, which was ranked with 0.45% of the area being affected by landslides. Furthermore, the formations of Pc, Jar-Jm-Js, Qm-Qp-al show a landslide activity of 0.32, 0.30 and 0.26%, respectively, which is equal to 0.48, 1.34 and 5.61% of the whole landslide activity area of the island. Low percentage of landslides reported as debris cones on coastal areas at the western part of the island, are shown in the geological units of Qc 0.017%, while no landsliding phenomena show are shown by the units of Tb-Tc. The detailed description of the geological units is provided in the caption of Fig. 1.

The statistical correlation of slope aspect with the location of slope failures depicts that almost all the landslides are concentrated in west-facing and southwest-facing slopes. In particular, the frequency of landslide activity in the former slopes is equal to 56%, while 40% is concentrated in the latter ones. Slopes located at the eastern part of the island show very low values of landslide density, where landslide

Table 1 Spatial distribution of geological units and relevant slope failure density

Geological unit	Surface area (km^2)	Surface area (%)	Unit landslide density	Total landslide density	Weight factor
Qm-Qp-al	27.43	9.03	0.26	5.62	− 0.47
Qt	1.63	0.54	0.17	0.21	− 0.93
Qc	15.52	5.11	0.02	0.20	− 3.23
M-Mgb-Mmg-Mb-Olm	61.29	20.17	0.10	4.86	− 1.42
E	48.32	15.9	0.11	4.20	− 1.33
Pc	1.94	0.64	0.32	0.48	− 0.29
C-Jc	22.63	7.45	0.12	2.17	− 1.23
Ci-Cs-Csd	30.29	9.97	2.18	51.21	1.64
Jar-Jm-Js	5.85	1.93	0.30	1.34	− 0.36
J1-J1d	86.14	28.34	0.45	29.85	0.05
Tb-Tc	2.56	0.84	0	0	0
Tg	0.35	0.12	0.08	0.02	− 1.7

Table 2 Spatial distribution of classes of slope aspect and relevant landslide density

Class	Aspect (°)	Class area (km^2)	Class area (%)	Class landslide density (%)	Total landslide density	Weight factor
1	0–40 north east	27.61	9.14	0.04	0.84	− 2.39
2	40–115 east	73.16	24.23	0.02	0.86	0.7
3	115–195 south east	63.88	21.15	0.03	1.45	− 2.68
4	195–275 south west	65.54	21.70	0.79	40.35	0.62
5	275–360 west	71.77	23.77	1.02	56.67	0.87

Table 3 Spatial distribution of classes of slope angles and relevant landslide density

Class	Slope angle (°)	Class area (km^2)	Class area (%)	Class landslide density (%)	Total landslide density	Weight factor
1	0–5	49.06	16.25	0.0008	0.03	− 6.26
2	5–10	52.48	17.38	0.0012	0.05	− 5.88
3	10–20	57.31	18.98	0.03	1.39	− 2.61
4	20–30	49.72	16.47	0.07	2.72	− 1.8
5	30–40	41.09	13.61	1.09	34.86	0.94
6	40–50	32.26	10.68	2.15	53.72	1.62
7	50–60	15.57	5.16	0.52	6.28	0.2
8	60–80	4.26	1.41	0.34	1.11	− 0.24
9	> 80	0.24	0.08	0	0	0

distribution does not exceed the 4% of the total activity area. The results of this analysis are listed in Table 2.

Papathanassiou et al. (2013) concluded that steeper slopes at the island of Lefkada had higher susceptibility to slope failures. This preliminary conclusion is verified by the statistical analysis of landslide activity in relation to the slope classes, as it is listed in Table 3. In particular, landslide activity is very frequent in slope angles higher than 30° while the highest density is related to slope angle between 40° and 50°, equals to 53.72%. The resulted spatial distribution in our study is in agreement with other earthquake-induced landslides cases, such as the 1989 Loma Prieta where landslides were mainly concentrated between 30° and 45° (Keefer 2000) and on slopes steeper than 27° regarding the 2004 Niigata earthquakes (Wang et al. 2007), as well as on slopes with angle between 45° and 60° (Kavoura and Sabatakakis 2019). In addition, according to Dou et al. (2019), the highest value of susceptibility ranges between 39° and 55°, considering the slope angle factor.

Finally, the correlation of spatial distribution of landslides with the elevation was investigated (Table 4). In particular, in the class of 0-300 m that covers only 48.84% of the study area, the landslide activity is 87.58% of the whole landslide activity in the island. It is followed by the unit of 300–600 m, that covers the 34.53% of the study area, which was ranked with 0.16% of the area being affected by landslides. Finally, the classes of 600–900 m and > 900 m did not show any landslide activity.

Based on the estimation of the total and unit/class landslide density per causal factor, the susceptibility to coseismic landslide was evaluated using the bivariate statistical analysis of Landslide Susceptibility Index (LSI). Considering the geology-oriented factor, the weight values that were estimated based on the Eq. (1) range between 1.64 for the unit of limestones of Paxos zone and − 3.23 for debris cones (Figs. 4a and 5a). The highest weight value that was assessed based on the slope angle map is equal to 1.62 for the class of slope angle 40°–50° and the lowest for the class of 0°–5°, equal to − 6.26 (Figs. 4b and 5b). The range of weight values of slope aspect map varies between 0.87 and − 2.68 (Figs. 4c and 5c), indicating that the significance of the factor to the triggering of landslides is not so important as the slope angle and the geology for this area. Finally, as it is shown in Figs. 4d and 5d, the highest weight value that was assessed based on the elevation map is equal to 0.58 for the class of 0–300 m elevation and the lowest for the class of 300–600 m elevation, equal to − 1.01.

The computed cumulative weight values per pixel of LSI range between 4.71 and − 13.18 for very high and very low susceptibility areas, respectively. For the purposes of this study, the resulting weight values map were initially normalized based on the natural breaks method and the equal interval method, and classified into 5 classes, representing Very High Susceptibility (VHS), High Susceptibility (HS), Moderate Susceptibility (MS), Low Susceptibility (LS), and Very Low Susceptibility (VLS). The area of the highest

Table 4 Spatial distribution of classes of elevation and relevant landslide density

Class	Elevation (m)	Class area (km^2)	Class area (%)	Class landslide density (%)	Total landslide density	Weight factor
1	0–300	147.5	48.84	0.77	87.58	0.58
2	300–600	104.26	34.53	0.16	12.59	− 1.01
3	600–900	37.13	12.30	0	0	0
4	> 900	13.1	4.34	0	0	0

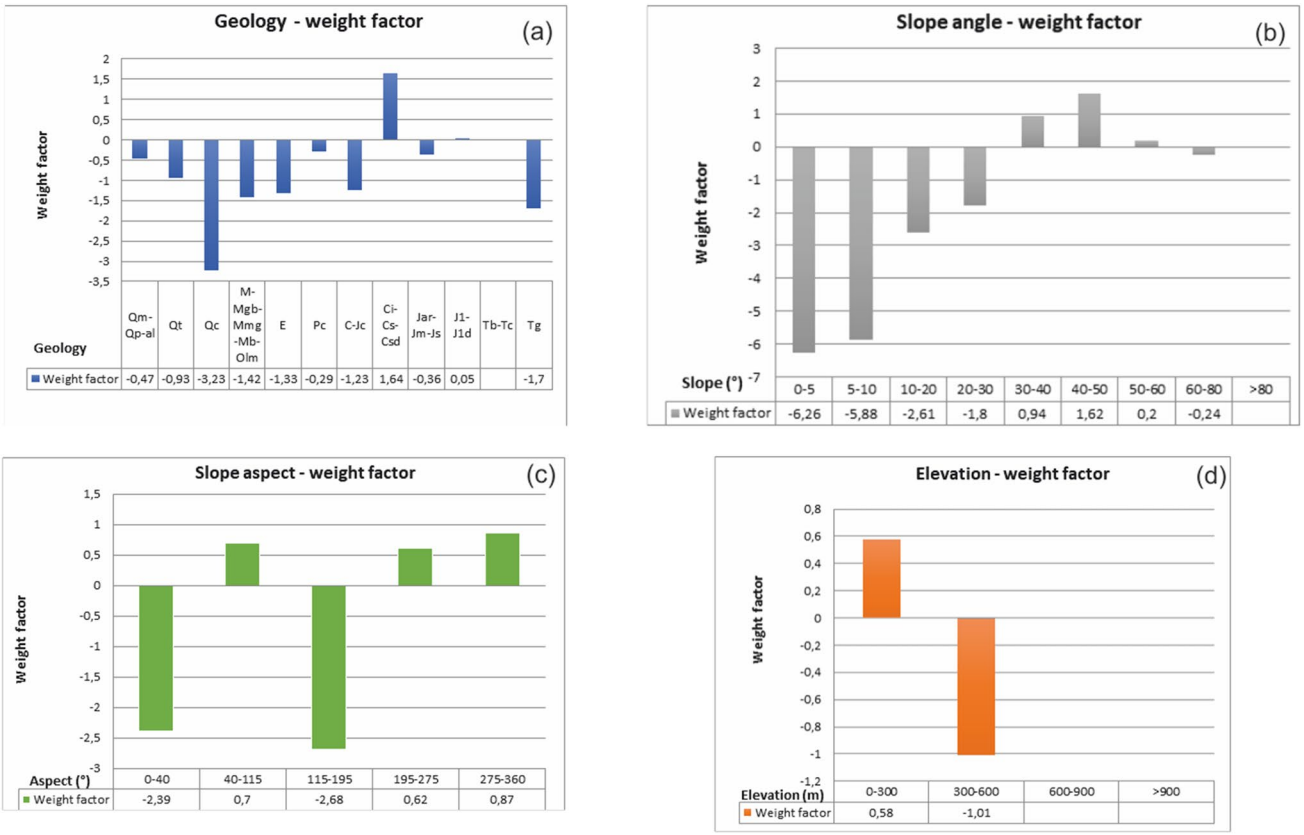

Fig. 4 **a** Weight factor values of classes of geological units ranging from 1.64 for the unit of limestones of Paxos zone to − 3.23 for debris cone, **b** Weight factor values of classes of slope angle ranging from 1.62 for the class of slope angle 40°–50° to the lowest for the class of 0°–5°, equal to − 6.26, **c** Weight factor values of classes of slope aspect ranging from 0.87 to − 2.68, **d** Weight factor values of classes of elevation ranging from 0.58 to − 1.01

susceptibility has been classified as "5", while the area of the lowest susceptibility was indicated as "1".

The results arisen by the application of these two methods are presented in the following sections while their performance is commented in the "Discussion" section. In addition, in this section is shown the developed coseismic landslide susceptibility maps based on the LSI and LR approaches. In particular, the accuracy of these methods (natural breaks and equal interval) was tested by splitting the dataset into two groups in order to be able to validate the relevant developed susceptibility maps; the set of slope failures of 2015 event was classified as the training set and the information provided by the inventory map of 2003 as the testing one. For the purposes of this study, the susceptibility map was validated by applying the approach of success rate and prediction rate curves (Dietrich et al. 1995; Chung and Fabbri 2003; Neuhäuser et al. 2011). The success rate curve assesses how many landslides sites are successfully captured by the susceptibility map, while the prediction rate curve shows the ability of the developed model to detect the likely to failure areas (van Westen et al. 2003; Neuhäuser et al. 2011; Kavoura and Sabatakakis 2019).

Natural breaks method (LSI analysis)

Having reclassified the LSI values based on the natural breaks method, a landslide susceptibility map was compiled and validated as it was previously presented. More specifically, it is shown that most of the landslide activity (79.8%) is concentrated within the area classified as "5", as well as the highest landslide activity per class is shown in class "5" (93.15%) (Fig. 6). In addition, the landslide activity within the three highest susceptibility areas is equal to 98% of the total activity, while the relevant activity within the two lowest susceptibility areas is less than 2%.

In order to examine the reliability of the model, we examined the slope of the first part of the predictive curve and the distance from the diagonal (Conforti et al. 2012). In our case, it is clearly shown that the first part of the curve is characterized as a high-sloping one, indicating a good performance of the model and thus, and a good reliability of the procedure including the selection of the causal factors. More specifically, the developed success rate curve shows that more than 70% of the slope failures are included within 10% of the susceptibility

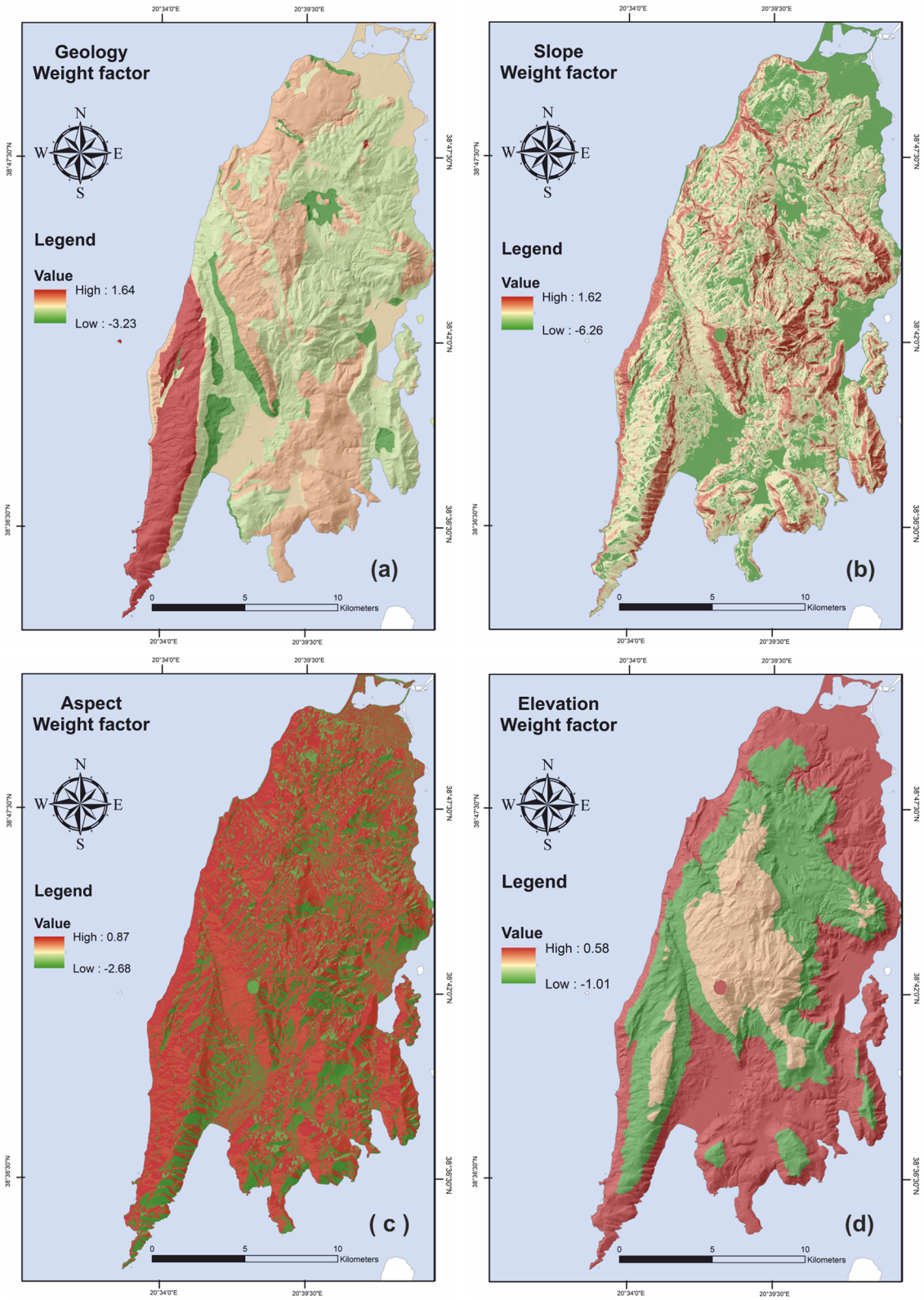

Fig. 5 Maps showing the distribution of the computed weight values of the **a** geological units, **b** slope angle classes, **c** slope aspect classes and **d** elevation classes

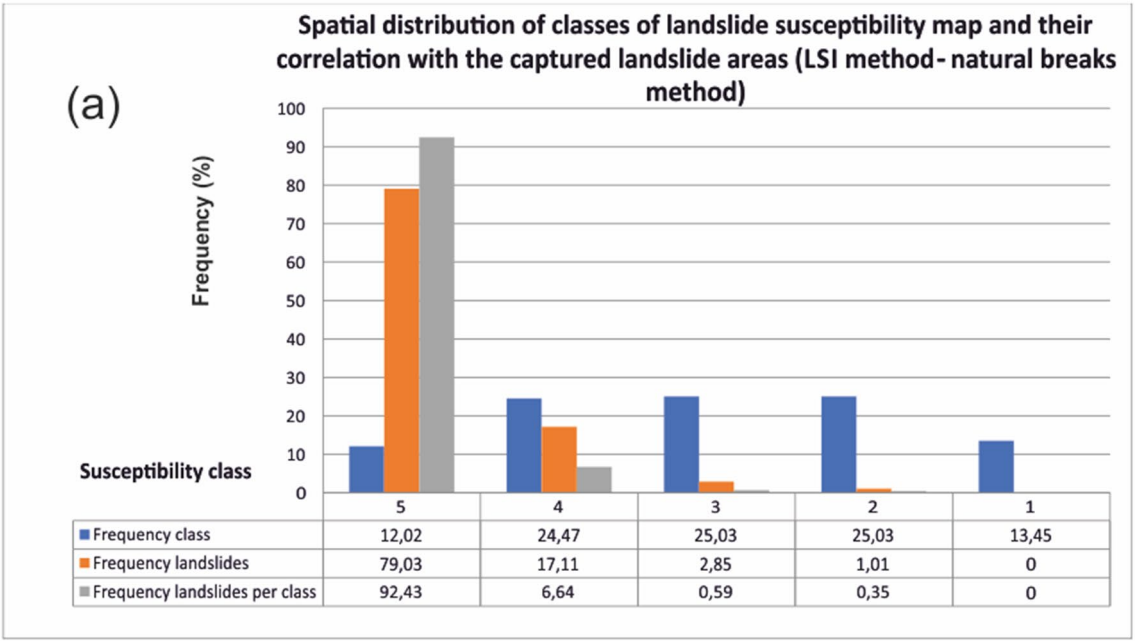

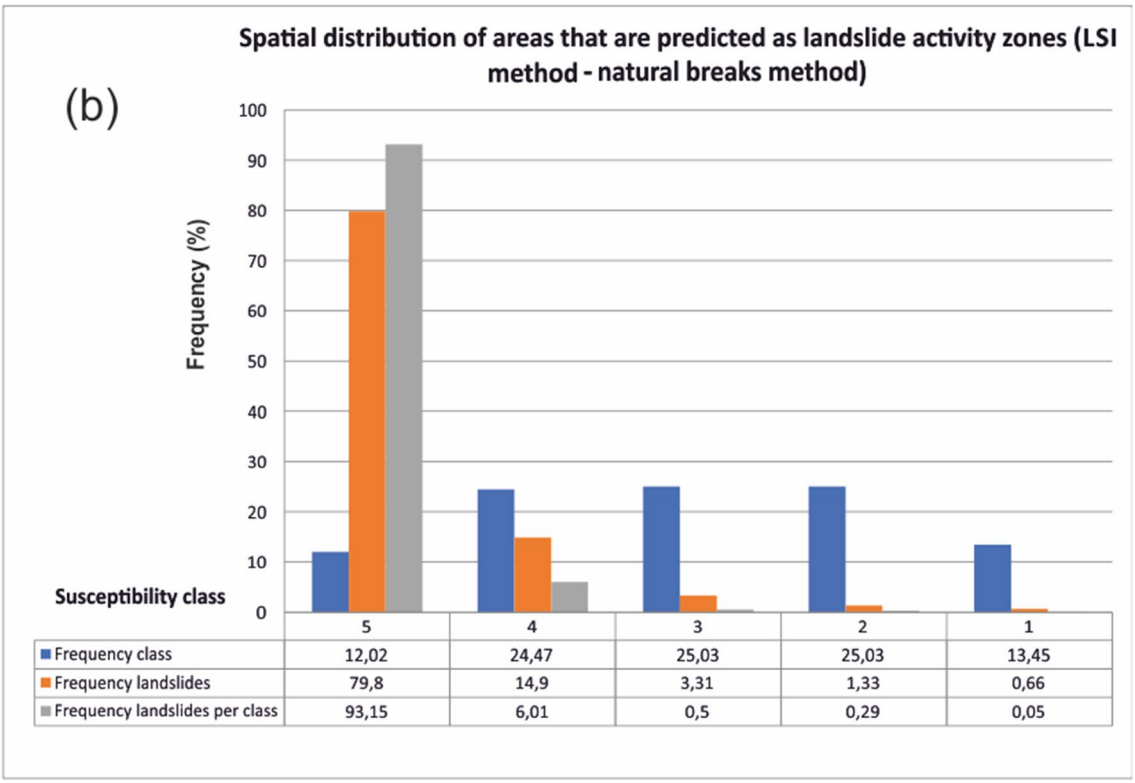

Fig. 6 **a** Spatial distribution of classes of landslide susceptibility map and their correlation with the captured landslide areas, **b** Spatial distribution of areas that are predicted as landslide activity zones

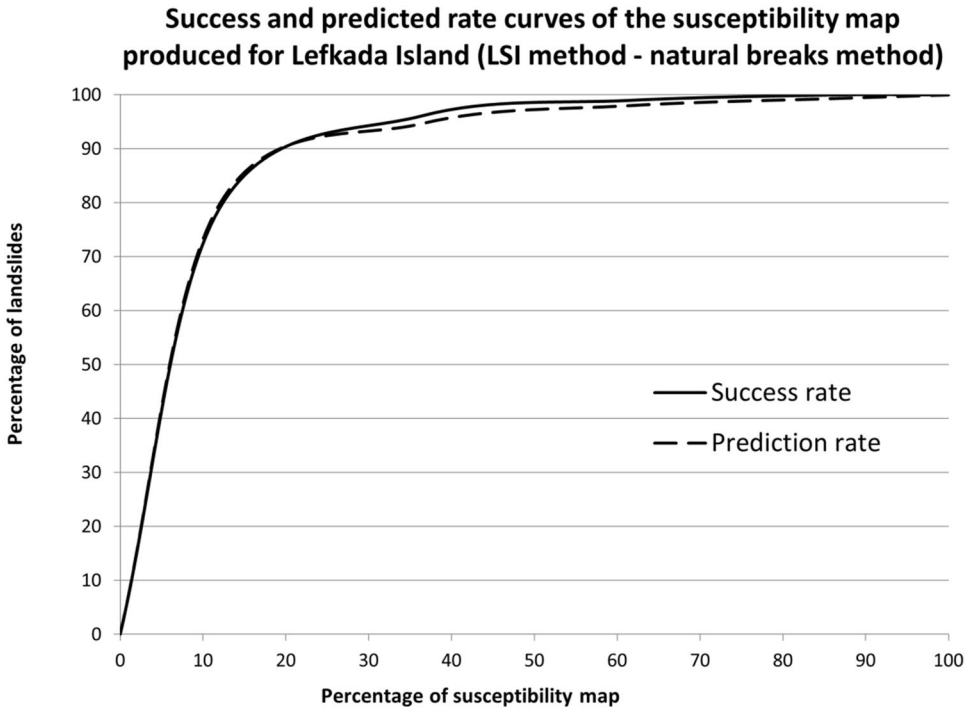

Fig. 7 Success and predicted rate curves of the susceptibility map produced for Lefkada Island, using the LSI method with the natural breaks method

map, while the prediction rate curve shows that more than 70% of landslides could be predicted at the same percentage of susceptibility units (Fig. 7). Another outcome arisen from this analysis is that 20% of the susceptibility map captures and predicts more than 90% of landslides.

Equal interval method (LSI analysis)

Following the similar approach, we examined the performance of the outcome arisen by the application of the equal interval method. As it is shown in Fig. 8, most of the landslide activity (65.56%) is concentrated within the area classified as "5", as well as the highest landslide activity per class is shown in class "5" (82.16%). In addition, the landslide activity within the three highest susceptibility areas is equal to 99.01% of the total activity, while the relevant activity within the two lowest susceptibility areas is less than 1%. The success rate curve shows that within 10% of the susceptibility map, 80% of the landslides are included (Fig. 9). At the same percentage of susceptibility units, the prediction rate curve shows that more than 70% of landslides could be predicted. Another outcome arisen from this analysis is that about 29% of the susceptibility map captures and predicts more than 90% of landslides.

Likelihood ratio

Furthermore, the susceptibility to coseismic landslides was additionally assessed based on the application of the LR. Considering the factor of geology, it can be observed in Table 5, Figs. 10a and 11a, that the highest likelihood ratio (4.33) has been attributed to the unit of limestones of Paxos zone, Ci-Cs-Csd formation. The classes namely Qc, Olm, and E have the lower likelihood ratios estimated as 0.2, 0.27, and 0.36, respectively. The highest value of LR for the slope aspect factor was estimated for the class of northwest-facing sloped, equal to 2.33 while the lowest value is related to the northeast-facing slopes (Table 6, Figs. 10c and 11c).

Considering the slope angle factor (Table 7, Figs. 10b and 11b), the highest values of LR are related to classes 60°–80° and 40°–50°, where the ratio was estimated at 21.51 and 13.46, respectively. Between these two classes, i.e. 50°–60°, the LR is also high 10.74, showing that high angle areas are highly susceptible to landslides. On the other hand, areas of low to medium slope angle are characterized by LR values range from 0.01 to 2.45 and can be classified as stable zones. The high values of LR indicate the influence of the slope angle parameter to the delineation of likely to coseismic landslides areas. Finally, regarding the factor of elevation, the areas located at an elevation between 0 and 300 m are showing the highest LR (1.58) (Table 8, Figs. 10d and 11d).

Afterwards, the summary of the likelihood ratio per pixel was computed and the values of LR values varied from 0 to 29.76. Similar to the procedure followed for the LSI method, for the purposes of this study, these values were reclassified into 5 classes of susceptibility by applying the natural breaks method and the equal interval method. In particular, the area of highest susceptibility has been classified as "5" while the area of lowest susceptibility was indicated as "1".

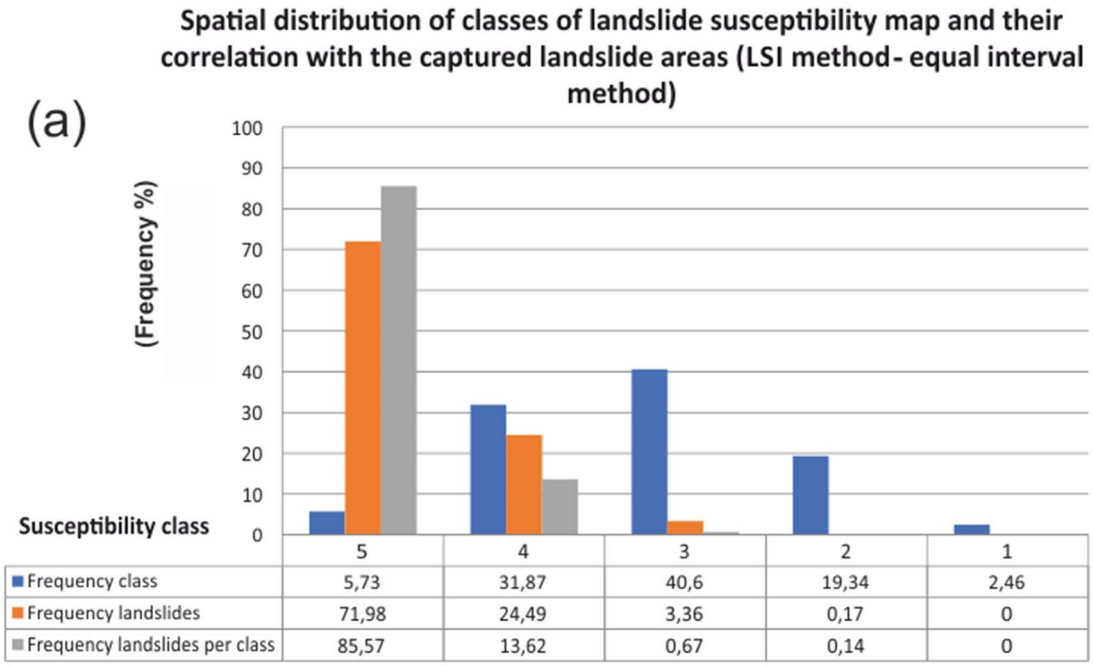

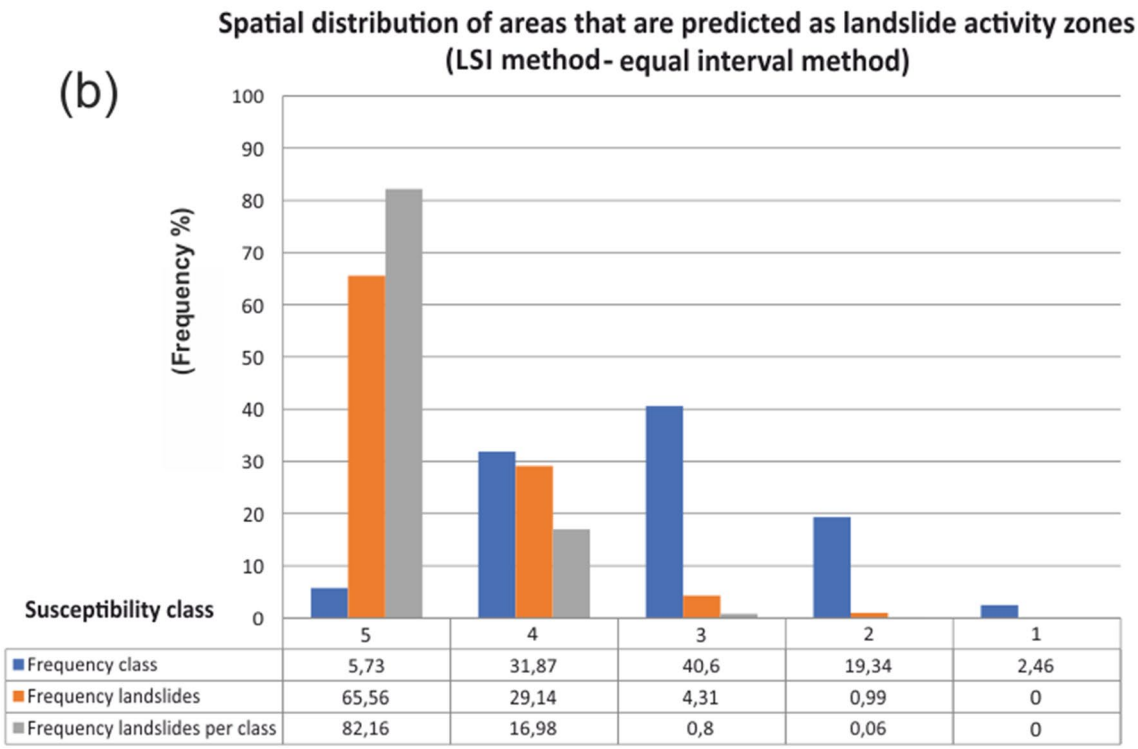

Fig. 8 **a** Spatial distribution of classes of landslide susceptibility map and their correlation with the captured landslide areas, **b** Spatial distribution of areas that are predicted as landslide activity zones

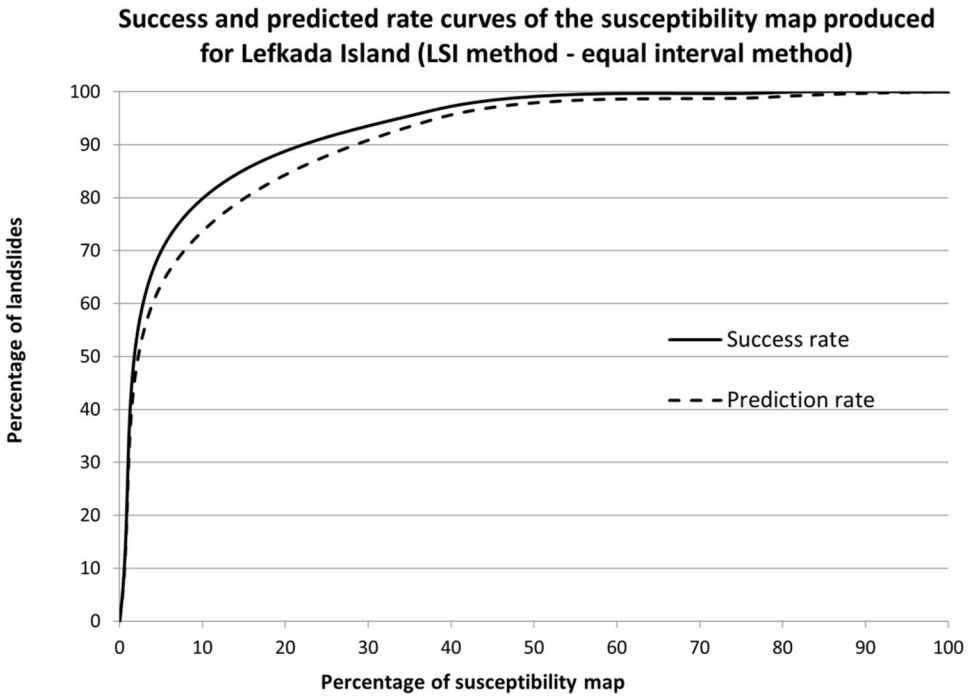

Fig. 9 Success and predicted rate curves of the susceptibility map produced for Lefkada Island, using the LSI method with the equal interval method

Table 5 Spatial distribution of geological units and relevant slope failure density—LR method

Class	Geological unit	Landslide frequency (occurrences)	Landslide frequency (%)	Class area (pixels)	Class area (%)	LR
1	Qm-Qp-al	38	6.38	27,433,534.32	9.03	0.71
2	Qt	2	0.34	1,626,695.377	0.54	0.63
3	Qc	6	1.01	15,521,567.33	5.11	0.2
4	M-Mgb-Mmg-Mb-Olm	32	5.37	61,285,094.67	20.16	0.27
5	E	34	5.71	48,317,698.42	15.9	0.36
6	Pc	2	0.34	1,937,606.094	0.64	0.53
7	C-Jc	34	5.71	22,638,094.21	7.45	0.77
8	Ci-Cs-Csd	257	43.12	30,301,534.41	9.97	4.33
9	Jar-Jm-Js	19	3.19	5,839,855.021	1.92	1.66
10	J1-J1d	171	28.69	86,155,422.35	28.34	1.01
11	Tb-Tc	0	0	2,564,967.293	0.84	0
12	Tg	1	0.17	348,467.6217	0.12	1.46

Natural breaks method (LR analysis)

The first approach that was applied for reclassifying the values of LR analysis, was the natural breaks method. According to this method, the percentage of landslide activity that is concentrated at the area classified as "5" is 58.28% (Fig. 12), while the relevant cumulative percentage within the two highest susceptibility classes is equal to 80%. Figure 13 depicts both the success and prediction rate curves that were calculated using the estimation and validation data set, respectively.

Regarding the equal interval method, it came out that the LR statistical analyses did not even fit the training dataset and for that reason we did not continue to test the validation dataset. The landslide frequencies were estimated as 1.68%, 30.20%, 17.28%, 36.58% and 14.26%, for the susceptibility classes "5" to "1", respectively, for the training set.

Discussion

The assessment of coseismic landslide susceptibility is considered as the first step for evaluating the relevant hazard within an area. In order to achieve this, several statistical approaches have been used by earth scientists, showing a

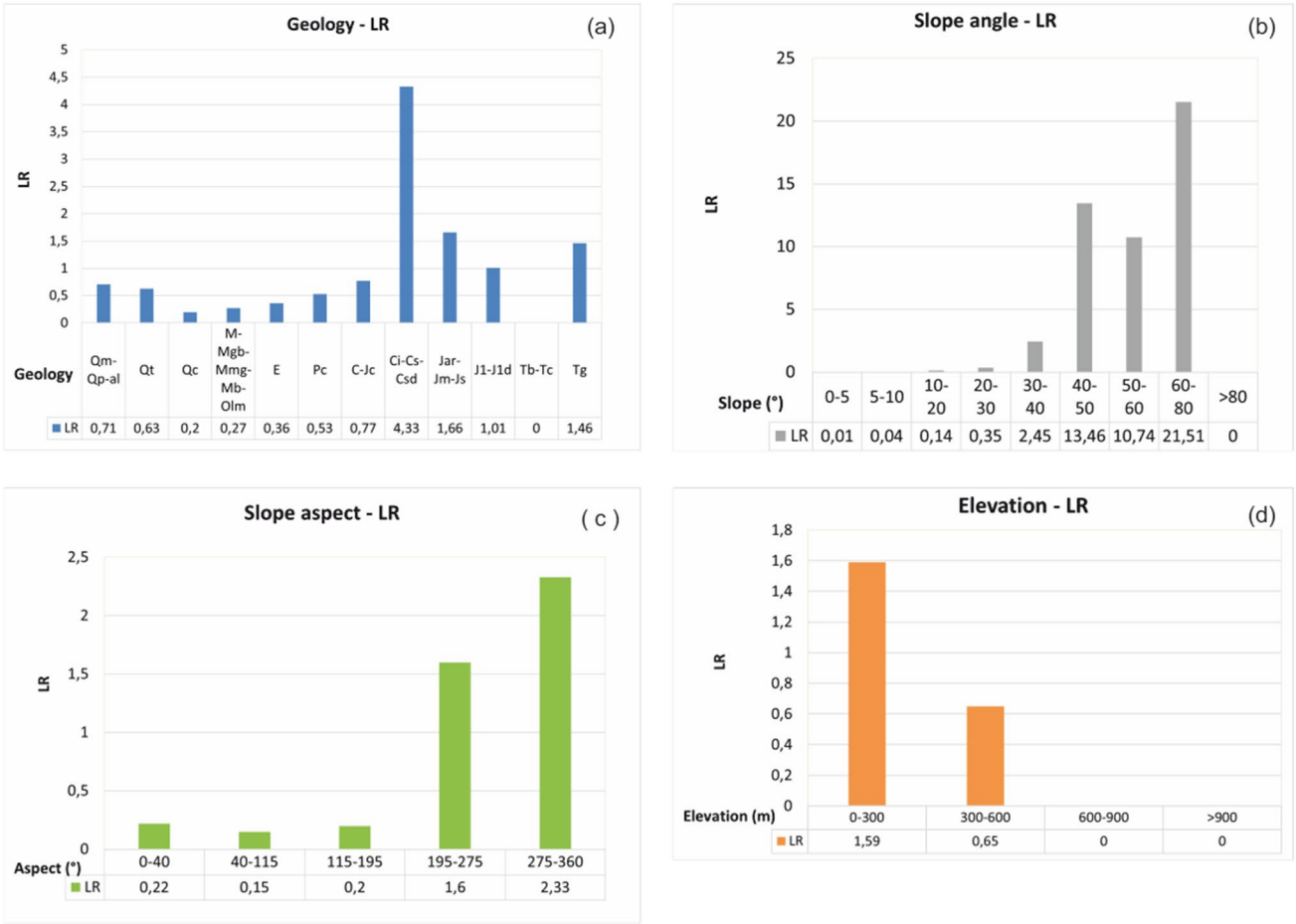

Fig. 10 **a** LR values of classes of geological units, **b** LR values of classes of slope angle, **c** LR values of classes of slope aspect and **d** LR values of classes of elevation

good correlation between the developed susceptibility map and the spatial distribution of slope failures. Among these methods, the Likelihood Ratio LR and the Landslide Susceptibility Index LSI have been chosen to be applied in the area of the island of Lefkada. This area is characterized by a high seismicity that triggers numerous slope failures causing severe structural damages to the manmade environment.

As regards both the Likelihood Ratio LR and the Landslide Susceptibility Index LSI, we have applied the natural breaks method and the equal interval method in order to reclassify the cumulative values per pixel. Taking into account the provided results, we concluded that applying the equal interval for the LSI, the prediction rate curve shows that more than 70% of landslides could be predicted at 10% of susceptibility units. Considering the natural breaks method, the developed success rate curve shows that more than 70% of the slope failures are included within 10% of the susceptibility map, while the prediction rate curve shows that more than 70% of landslides could be predicted at the same percentage of susceptibility units. Another outcome arisen from this analysis is that 20% of the susceptibility map captures and predicts more than 90% of landslides.

Considering the LR method, the natural breaks method shows the best performance since the success rate curve indicates that 80% of the landslides are included within 10% of the susceptibility map, while at the same percentage of susceptibility units, the prediction rate curve shows that more than 76% of landslides could be predicted. The equal interval method did not even fit the training dataset for the LR method.

Thus, we took into account the natural breaks method in order to develop the coseismic landslide susceptibility maps in the island of Lefkada (Figs. 14 and 15) based on the LSI and LR method, respectively.

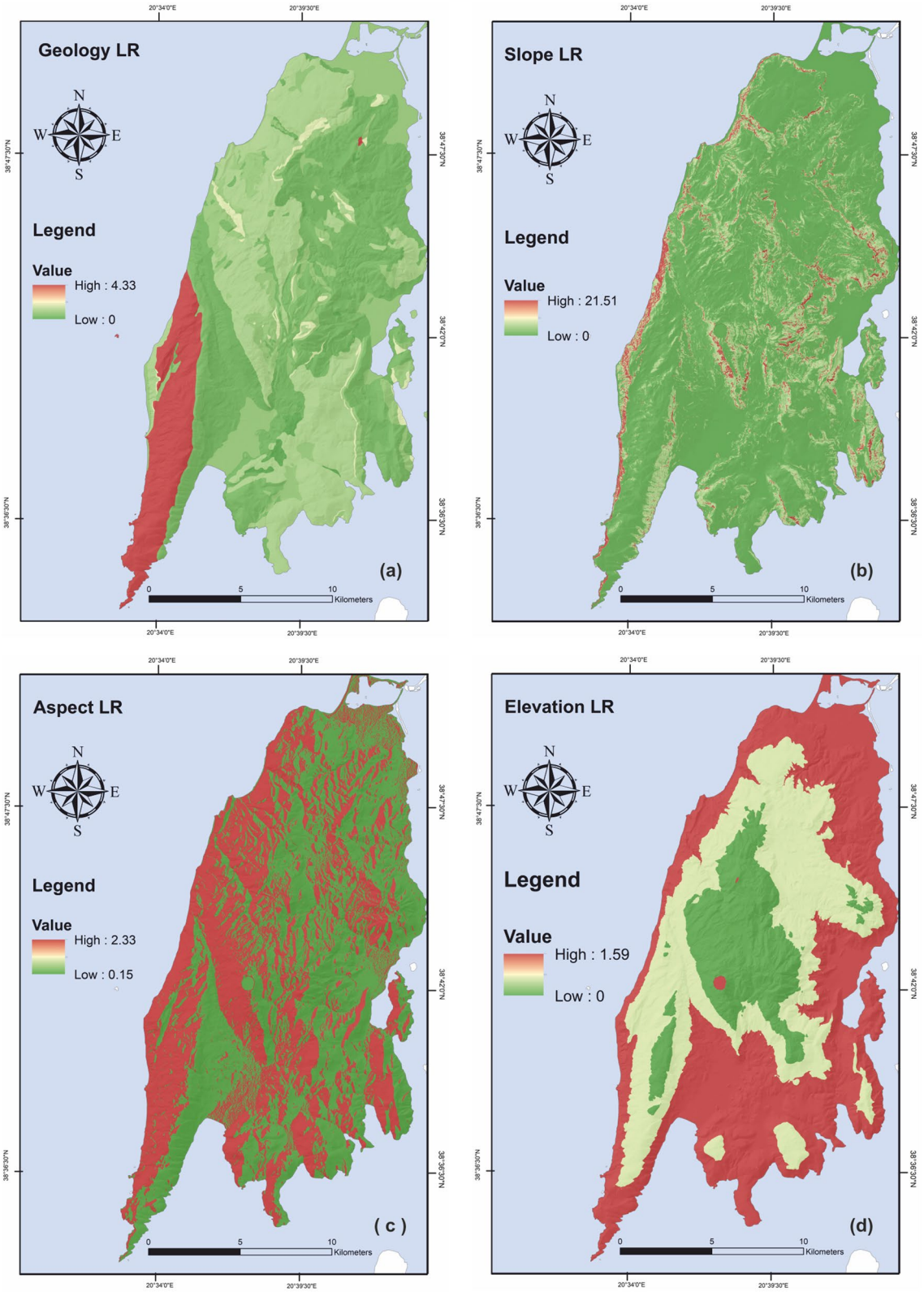

Fig. 11 **a** Map showing the distribution of the computed LR values of the geological units, **b** Map showing the distribution of the computed LR values of the slope angle classes, **c** Map showing the distribution of the computed LR values of the slope aspect classes, and **d** Map showing the distribution of the computed LR values of the elevation classes

Table 6 Spatial distribution of classes of slope aspect and relevant landslide density—LR method

Class	Aspect (°)	Landslide frequency (occurrences)	Landslide frequency (%)	Class area (pixels)	Class area (%)	LR
1	0–40	12	2.01	27,609,657.17	9.14	0.22
2	40–115	22	3.69	73,155,627.85	24.23	0.15
3	115–195	25	4.2	63,877,366.87	21.15	0.2
4	195–275	207	34.73	65,544,406.28	21.71	1.6
5	275–360	330	55.37	71,772,652.17	23.77	2.33

Table 7 Spatial distribution of classes of slope angles and relevant landslide density—LR method

Class	Slope angle (°)	Landslide frequency (occurrences)	Landslide frequency (%)	Class area (pixels)	Class area (%)	LR
1	0–5	1	0.17	42,886,433.63	14.2	0.01
2	5–10	3	0.5	35,949,905.42	11.91	0.04
3	10–20	24	4.03	89,916,269.13	29.78	0.14
4	20–30	52	8.73	76,247,166.43	25.25	0.35
5	30–40	220	36.91	45,561,824.58	15.09	2.45
6	40–50	248	41.61	9,337,459.843	3.09	13.46
7	50–60	36	6.04	1,698,320.658	0.56	10.74
8	60–80	12	2.01	282,626.8275	0.09	21.51
9	> 80	0	0	90,706.4792	0.03	0

Table 8 Spatial distribution of classes of elevation and relevant landslide density—LR method

Class	Elevation (m)	Landslide frequency (occurrences)	Landslide frequency (%)	Class area (pixels)	Class area (%)	LR
1	0–300	462	77.52	147,496,520.2	48.84	1.59
2	300–600	134	22.48	104,261,442.3	34.53	0.65
3	600–900	0	0	37,130,475.02	12.3	0
4	> 900	0	0	13,101,895.23	4.34	0

Considering the former approach, i.e. LSI, the developed landslide susceptibility map is shown in Fig. 14a. The areas classified as moderate, high and very high cover almost the 62% of the total area while the landslide activity within these areas is equal to almost 99% of the total activity. Furthermore, a qualitative correlation of the spatial distribution of the susceptibility classes with the local road network in the island has been investigated by overlaying the relevant layers (Fig. 14b). In this figure, the susceptibility classes very low "1" and low "2" have been grouped within one class, so the correlation among the three highest susceptibility classes moderate "3", high "4" and very high "5" with the road network and the settlements could be clearly presented to the reader.

Analyzing the spatial distribution of the susceptibility classes, developed based on the LR method (Fig. 15a), it is

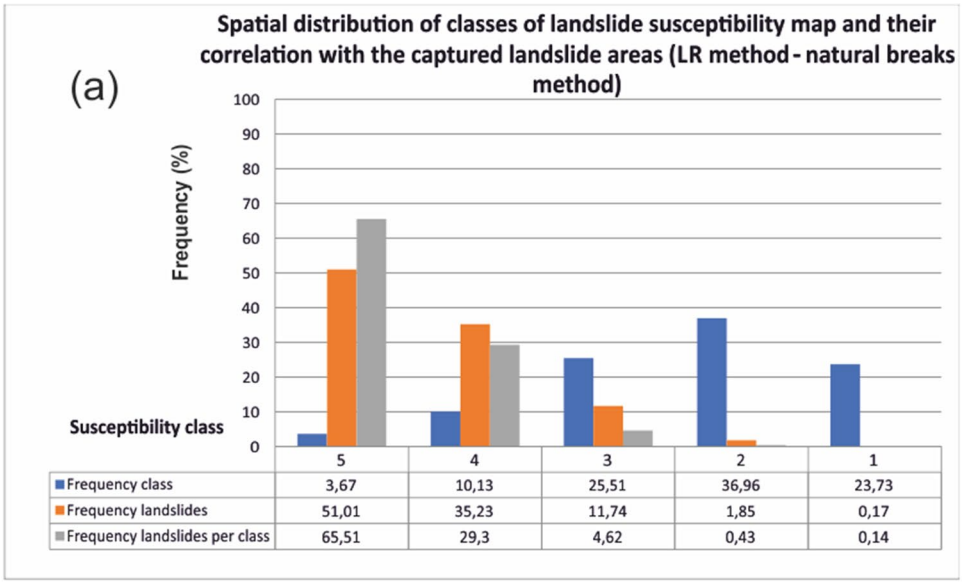

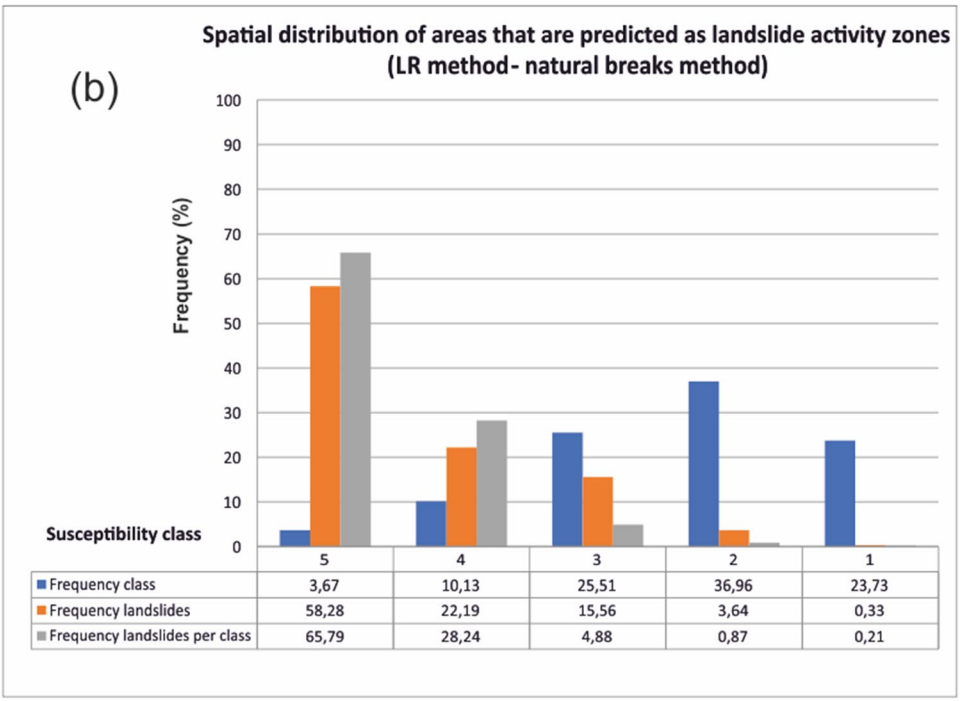

Fig. 12 **a** Spatial distribution of classes of landslide susceptibility map and their correlation with the captured landslide areas with LR method, and **b** Spatial distribution of areas that are predicted as landslide activity zones, with LR method

shown that the highest susceptibility area that is classified as "5" covers the 3.67% of the total study area, and the lowest susceptibility area, classified as "1", covers the 23.73% of the study area. In addition, the layers of the spatial distribution of the road network and the location of the villages were correlated with the relevant layer of the susceptibility classes (Fig. 15b).

The outcome arisen by the application of both approaches (LSI and LR), is that the western coastal part of the Lefkada island is characterized by high and very high susceptibility

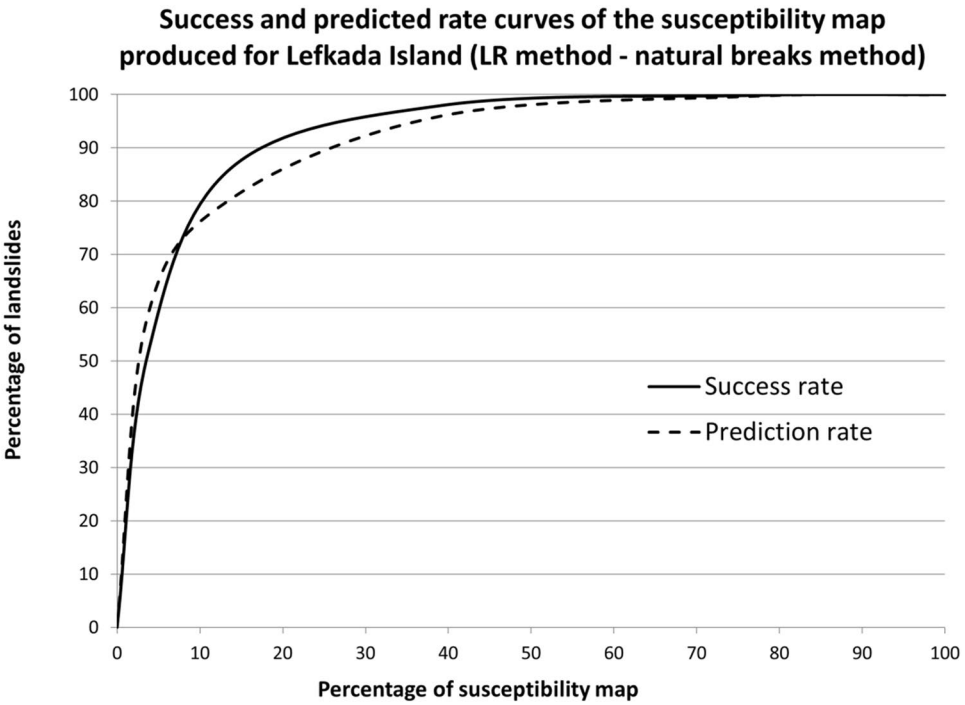

Fig. 13 Success and predicted rate curves of the susceptibility map produced for Lefkada Island, with LR method with natural breaks method. The success rate curve shows that within 10% of the susceptibility map, 80% of the landslides are included. At the same percentage of susceptibility units, the prediction rate curve shows that more than 76% of landslides could be predicted

while the northern part of the island (wider area of the Lefkada town) is characterized by very low and low susceptibility. Nevertheless, there are some differences on the results of these approaches. In particular, the LR model provides a coarser susceptibility map where the central part of the island is mainly characterized by very low susceptibility, whereas on the LSI model the classification of the susceptibility is more detailed, mainly representing medium susceptibility classes. Although the fact that both developed maps are considered as reliable regarding the delineation of coseismic landslides, the map compiled based on the Likelihood Ratio (LR) with the natural breaks method seems to provide a slightly better performance regarding the percentage of landslides that could be forecasted at the same percentage of susceptibility units; 76% and 70% based on the LR and LSI, respectively.

Considering the classification of geological units, the one of limestones of Paxos zone presents the highest susceptibility on both models. The classification of slope angle on LR model highlights the influence of high-angle slopes and is considered as the most crucial for the triggering of coseismic landslides. However, based on the LSI model, the highest susceptibility is observed on slope angles of 40°–50°, whereas on the LR model this classification is related to the class of 60°–80°. Regarding the factor of slope aspect, it is resulted on both models that the northwest-facing slopes are considered as the most susceptible to fail.

Correlating the road network with the spatial distribution of susceptibility, it is shown that considering the LSI method, the class "3" includes 24.88%, the class "4" includes 21.38% and the class of highest susceptibility "5" only 7.22% of the total road network. As for the LR method, it came out that class "3" includes 23.84%, class "4" includes 8.42% and the class of highest susceptibility "5" includes 1.47% of the total network (Table 9). Based on the outcome of this correlation, it is clear to the authorities which roads will face problems due to an earthquake, facilitating the post-seismic response and the taken actions focusing on the delivery of aid.

Furthermore, regarding the location of settlements and the relevant susceptibility, some differences are observed. More specifically, settlements characterized by high susceptibility based on the LSI method (e.g. Exanthia, Alatron, Marantohori and Evgiros), present medium to low susceptibility in LR method. (Table 10).

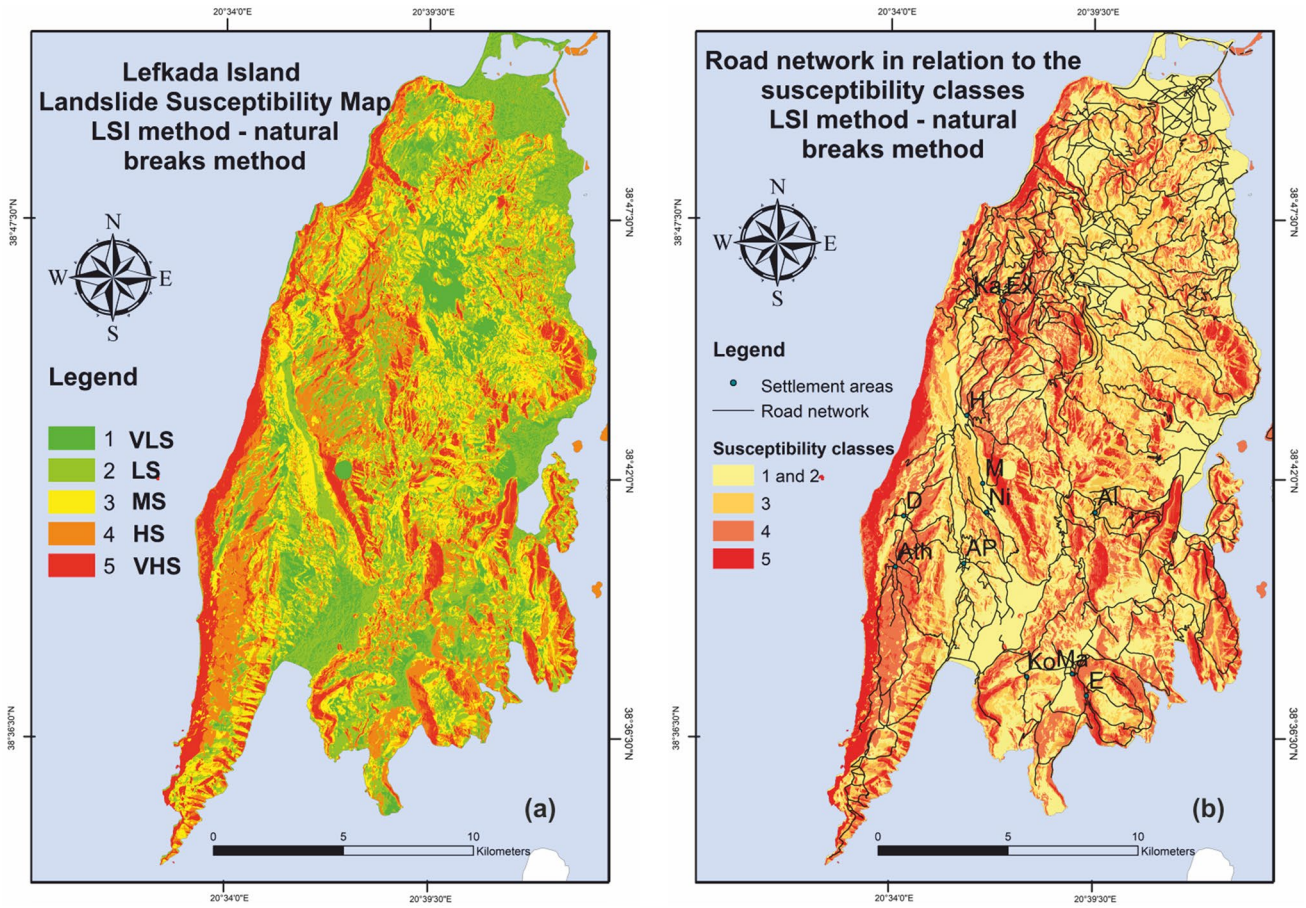

Fig. 14 **a** Lefkada Island coseismic landslide susceptibility map developed based on the LSI method with the natural breaks method. From 1 to 5 are indicated the landslide susceptibility classes; the 1st class represents very low susceptibility (VLS), whereas the 5th class represents very high susceptibility (VHS). The three most susceptible classes, classified as "3", "4," and "5", cover almost the 62% of the total area, while the landslide activity within these areas is equal to almost 99% of the total activity, **b** The map showing the road network and the settlements (ID listed in Table 10) in the Lefkada Island in relation to the susceptibility classes. The outcome provided by this study is that 194 km and 240 m of the road network are in the area classified as "3" while 166 km and 890 m and 56 km and 390 m, in the areas "4" and "5," respectively

Conclusions

The island of Lefkada, Greece is considered as one of the most seismically active areas in Europe where moderate events frequently occurred. The predominant secondary effects are slope failures-related phenomena, i.e. rockfalls, rock slides, and are mainly reported on the western part of the island. The last 20 years, two events occurred in 2003 and 2015 and relevant coseismic landslide inventories were compiled. Based on the information provided by these inventories, i.e. spatial distribution of slope failures, this study aims to develop an updated earthquake-induced landslide map; the first version was compiled by Papathanassiou et al. (2013). This was achieved by statistically analysing, based on the approaches of Landslide Susceptibility Index and Likelihood Ratio, the distribution of predisposing factors, i.e. geology, slope angle, slope aspect and elevation with the location of slope failures.

In particular, following the statistical analyses, it was shown that the highest frequency of landslides is related

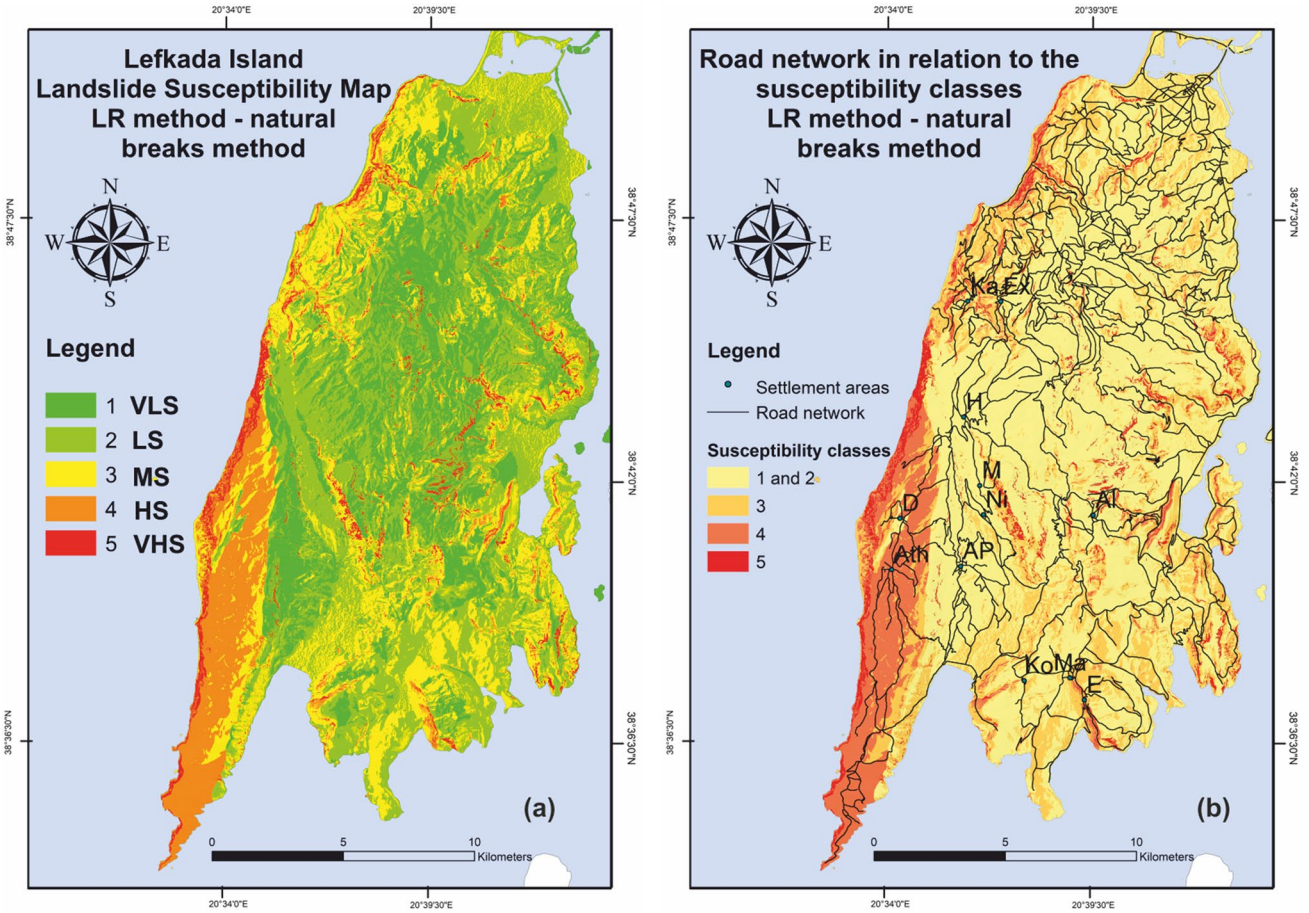

Fig. 15 **a** Lefkada Island coseismic landslide susceptibility map developed based on the LR method, with the natural breaks method. From 1 to 5 are indicated the landslide susceptibility classes; the 1st class represents very low susceptibility (VLS), whereas the 5th class represents very high susceptibility (VHS). The most susceptible class areas, classified as "4", and "5," cover the 13% of the total area, while the landslide activity within these areas is equal to almost 86% of the total activity, **b** Map showing the road network and the settlement areas (ID listed in Table 10) in the Lefkada Island

Table 9 Comparative table depicting the correlation of the road network with the spatial distribution of susceptibility, for LSI and LR methods, respectively

	Susceptibility classes	Length of road network (km)	Road network (%)
LSI method	1 and 2	363.19	46.52
	3	194.24	24.88
	4	166.89	21.38
	5	56.39	7.22
LR method	1 and 2	517.38	66.27
	3	186.12	23.84
	4	65.77	8.42
	5	11.44	1.47

with the geological formation of limestones of Paxos zone and with northwest-facing slopes. Considering the factor of slope angle, the LSI-based method shows that the highest frequency of slope failures is related to slope angles between 40° and 50°, while the LR approach indicates the areas of high angle slopes (60°–80°) as the most susceptible.

The validation of the susceptibility map was achieved by using the dataset of the coseismic landslide inventory of 2003 event and more specifically by comparing and statistically analysing the developed susceptibility maps with the spatial distribution of slope failures triggered by the 2003 earthquake. The outcome arisen by the LSI-based analysis indicates that the prediction rate curve could predict more than 70% of the landslides within 10% of the susceptibility map, while 20% of the susceptibility map predicts more than 90% of landslides. In LR model, the prediction rate curve shows that more than 76% of landslides could be predicted within 10% of the susceptibility map.

Table 10 Comparative table depicting the location of settlements and the relevant susceptibility

Name	ID	LSI method Susceptibility class	LR method Susceptibility class
Kalamitsi	Ka	1	1
Exanthia	Ex	3	2
Hortata	Ho	2	1
Manasi	Ma	2	2
Nikolis	Ni	2	2
Alatron	Al	3	2
Agios Petros	AP	2	1
Dragano	Dr	3	3
Athanio	At	4	4
Kontaraina	Ko	3	2
Marantohori	Mr	4	3
Evgiros	Ev	4	3

As an outcome, these maps highlight the likely to earthquake-induced slope failures areas in the island of Lefkada and accurately points out the segments of the road network that are in the most susceptible landslides zones. The latter conclusion is believed to be a crucial parameter for the emergency response efforts after an earthquake since based on this map the authorities can assess in advance the roads that can be disrupted due to the occurrence of coseismic slope failures.

Acknowledgements We would like to thank the three anonymous reviewers for their constructive comments.

Funding Not applicable.

Availability of data and material Not applicable.

Code availability Not applicable.

Declarations

Conflict of interest The authors declare no conflict of interest.

References

Ayalew L, Kasahara M, Yamagishi H (2011) The spatial correlation between earthquakes and landslides in Hokkaido (Japan), a GIS-based analysis of the past and the future. Landslides 8:443–448

B. P. Co ltd (1971) The geological results of petroleum exploration in Western Greece. Special report 10. Institute of Geology and Subsurface Research, Athens

Baeza C, Lantada N, Moya J (2010) Validation and evaluation of two multivariate statistical models for predictive shallow landslide susceptibility mapping of the Eastern Pyrenees (Spain). Environ Earth Sci 61(3):507–523

Bird JF, Bommer JJ (2004) Earthquake losses due to ground failure. Eng Geol 75(2):147–179. https://doi.org/10.1016/j.enggeo.2004.05.006

Bonham-Carter GF (1994) Geographic information systems for geoscientist: modeling with GIS. Pergamon, New York, pp 302–334

Bornovas J (1964) Géologie de l'île de Lefkade. Geol Geoph Res 10

Brabb E (1984) Innovative approaches to landslide hazard and risk mapping. Proc Fourth Int Symp Landslides 1:307–323

Caporali A, Bruyninx C, Fernandes R, Ganas A, Kenyeres A, Lidberg M (2016) Stress drop at the Kephalonia Transform Zone estimated from the 2014 seismic sequence. Tectonophysics 666:164–172

Chalkias Ch, Ferentinou M, Polykretis Ch (2014) GIS-Based Landslide Susceptibility Mapping on the Peloponnese Peninsula, Greece. Geosciences. https://doi.org/10.3390/geosciences4030176

Chigira M, Yagi H (2006) Geological and geomorphological characteristics of landslides triggered by the 2004 Mid Niigata prefecture earthquake in Japan. Eng Geol. https://doi.org/10.1016/j.enggeo.2005.10.006

Chung CJF, Fabbri A (2003) Validation of spatial prediction models for landslide hazard mapping. Nat Hazard 30:451–472

Chung CJ, Fabbri A, van Westen CJ (1995) Multivariate regression analysis for landslide hazard zonation. In: Carrara A, Guzetti F (eds) Geographical information systems in assessing natural hazards. Kluwer, pp 107–133

Clement C, Hirn A, Charvis P (2000) Seismic structure and the active Hellenic subduction in the Ionian islands. Tectonics 329(1–4):141–156

Conforti M, Robustelli G, Muto F, Critelli S (2012) Application and validation of bivariate GIS-based landslide susceptibility assessment for the Vitravo river catchment (Calabria, south Italy). Nat Hazard 61:127–141

Cui P, Chen X-Q, Zhu Y-Y, Su F-H, Wei F-Q, Han Y-S, Liu H-J, Zhuang J-Q (2009) The Wenchuan Earthquake (May 12, 2008), Sichuan Province, China, and resulting geohazards. Nat Hazards 56:19–36. https://doi.org/10.1007/s11069-009-9392-1

Cushing EM (1985) Evolution sructurale de la marge nord-ouest hellenique dans l' ile de Levkas et ses envinors (Grece nord-occidentale), Université de Paris-Sud. Faculté des sciences d'Orsay (Essonne)

Dai FC, Lee CF (2002) Landslide characteristics and slope instability modeling using GIS, Lantau Island, Hong Kong. Geomorphology 42:213–228. https://doi.org/10.1016/S0169-555X(01)00087-3

Dellow S, Massey C, Cox S, Archibald G, Begg J, Bruce Z, Carey J, Davidson J, Pasqua FD, Glassey P, Hill M, Jones K, Lyndsell B, Lukovic B, McColl S, Rattenbury M, Read S, Rosser B, Singeisen C, Townsend D, Villamor P, Villeneuve M, Godt J, Jibson R, Allstadt K, Rengers F, Wartman J, Rathje E, Sitar N, Adda A-Z, Manousakis J, Little M (2017) Landslides caused by the Mw7.8 Kaikōura earthquake and the immediate response. Bull N Z Soc Earthq Eng 50(2):106–116. https://doi.org/10.5459/bnzsee.50.2.106-116

Dietrich EW, ReissR HML, Montgomery DR (1995) A process-based model for colluvial soil depth and shallow landsliding using digital elevation data. Hydrol Process 9:383–400

Dou J, Yunus AP, Tien Bui D, Sahana M, Chen CW, Zhu Zh, Wang W, Thai Pham B (2019) Evaluating GIS-based multiple statistical models and data mining for earthquake and rainfall-induced landslide susceptibility using the LiDAR DEM. Remote Sens 11:638. https://doi.org/10.3390/rs11060638

Duman TY, Can T, Gokceoglu C, Nefeslioglu HA, Sonmez H (2006) Application of logistic regression for landslide susceptibility zoning of Cekmece Area, Istanbul, Turkey. Environ Geol 51:241–256

Ercanoglu M, Gokceoglu C (2004) Use of fuzzy relations to produce landslide susceptibility map of a landslide prone area (West Black Sea Region, Turkey). Eng Geol 75:229–250. https://doi.org/10.1016/j.enggeo.2004.06.001

Ganas A, Marinou A, Anastasiou D, Paradissis D, Papazissi K, Tzavaras P, Drakatos G (2013) GPS-derived estimates of crustal deformation in the central and north Ionian Sea, Greece: 3-yr results from NOANET continuous network data. J Geod 6:62–71

Ganas A, Elias P, Bozionelos G, Papathanassiou G, Avallone A, Papastergios A, Valkaniotis S, Parcharidis I, Briole P (2016) Coseismic deformation field observations and seismic fault of the 17 November 2015 M=6.5, Lefkada Island, Greece earthquake. Tectonics 687:210–222 (ISSN 0040–1951). https://doi.org/10.1016/jtecto.2016.08.012.

Grendas N, Marinos V, Papathanassiou G, Ganas A, Valkaniotis S (2018) Engineering geological mapping of earthquake-induced landslides in South Lefkada Island, Greece: evaluation of the type and characteristics of the slope failures. Environ Earth Sci 77:425. https://doi.org/10.1007/s12665018-7598-9

Guirong W, Xi Ch, Wei Ch (2020) Spatial prediction of landslide susceptibility based on GIS and discriminant functions. Int J Geo Inf 9:144. https://doi.org/10.3390/ijgi9030144

Guzzetti F, Carrara A, Cardinali M, Reichenbach P (1999) Landslide hazard evaluation: a review of current techniques and their application in a multi-scale study, Central Italy. Geomorphology 31:181–216

Hatzfeld D, Kassaras I, Panagiotopoulos D, Amorese D, Makropoulos K, Karakaisis GF, Coutant O (1995) Microseismicity and strain pattern in Northwestern Greece. Tectonics 14:773–785

He S, Pan P, Dai L, Wang H, Liu J (2012) Application of kernel-based Fisher discriminant analysis to map landslide susceptibility in the Qinggan River delta, Three Gorges, China. Geomorphology 171–172:30–41

Hikima K, Koketsu K (2005) Rupture processes of the 2004 Chuetsu (mid-Niigata prefecture) earthquake, Japan: a series of events in a complex fault system. Geophys Res Lett 32:L18303. https://doi.org/10.1029/2005GL023588

Huiming T, Hongbiao J, Xinli H, Dewei L, Chengren X (2010) Characteristics of landslides induced by the great Wenchuan Earthquake. J Earth Sci 21(1):104–113. https://doi.org/10.1007/s12583-010-0008-1

Ilieva M, Briole P, Ganas A, Dimitrov D, Elias P, Mouratidis A, Charara R (2016) Fault plane modelling of the 2003 August 14 Lefkada Island (Greece) earthquake based of the analysis of ENVISAT SAR interferograms. Tectonics 693:47–65

Imanishi K, Kuwahara Y, Takeda T, Haryu Y (2006) The seismicity, fault structures, and stress field in the seismic gap adjacent to the 2004 Mid-Niigata earthquake inferred from seismological observations. Earth Planet Space 58:831–841. https://doi.org/10.1186/BF03351988

Jessee N, Hamburger MW, Allstadt K, Wald DJ, Robeson SM, Tanyas H, Hearne M, Thompson EM (2018) A global empirical model for near-real-time assessment of seismically induced landslides. J Geophys Res Earth Surf 123:1835–1859. https://doi.org/10.1029/2017JF004494

Jibson RW, Harp EL, Michael JA (2000) A method for producing digital probabilistic seismic landslide hazard maps. Eng Geol 58:271–289

Kanungo DP, Sarkar S, Sharma S (2011) Combining neural network with fuzzy, certainty factor and likelihood ratio concepts for spatial prediction of landslides. Nat Hazards 59:1491–1512. https://doi.org/10.1007/s11069-011-9847-z

Kavoura K, Sabatakakis N (2019) Investigating landslide susceptibility procedures in Greece, vol 17. Springer, pp 127–145. https://doi.org/10.1007/s10346-019-01271-y

Kazantzidou-Firtinidou D, Kassaras I, Tonna S, Ganas A, Vintzileou E, Chesi C (2016) The November 2015 Mw 6.4 earthquake effects in Lefkas Island. In: 1st International Conference on Natural Hazards & Infrastructure, 28–30 June 2016, Chania

Keefer DK (1984) Landslides caused by earthquakes. Geol Soc Am Bull 95(4):406–421. https://doi.org/10.1130/0016-7606(1984)95%3c406:lcbe%3e2.0.co;2

Keefer DK (2000) Statistical analysis of an earthquake-induced landslide distribution- the 1989 Loma Prieta California event. Eng Geol 58:213–249

Kiernan G (2016) Repairing Kaikoura: the size, the speed, and the cost of delays, posted on Infometrics. https://www.infometrics.co.nz/repairing-kaikoura-size-speed-cost-delays/

Lee S (2004) Application of likelihood ratio and logistic regression models to landslide susceptibility mapping using GIS. Environ Manage 34:223–232. https://doi.org/10.1007/s00267-003-0077-3

Lee S (2007) Comparison of landslide susceptibility maps generated through multiple logistic regression for three test areas in Korea. Earth Surf Process Landf 32:2133–2148. https://doi.org/10.1002/esp.1517

Lekkas E, Mavroulis S, Alexoudi V (2016) Field observations of the 2015 (November 17, MW 6.4) Lefkas (Ionian sea, Western Greece) earthquake impact on natural environment and building stock of Lefkas island. Bulletin of the Geological Society of Greece, vol, pp 499–510. In: Proceedings of the 14th International Congress, Thessaloniki, May 2016

Lombardo L, Mai PM (2018) Presenting logistic regression-based landslide susceptibility results. Elsevier 0013-7952/, https://doi.org/10.1016/j.enggeo.2018.07.019.

Louvari E, Kiratzi A, Papazachos BC (1999) The CTF and its extension to western Lefkada Island. Tectonophysics 308:223–236

Marano KD, Wald DJ, Allen TI (2009) Global earthquake casualties due to secondary effects: a quantitative analysis for improving rapid loss analyses. Nat Hazards 52(2):319–328. https://doi.org/10.1007/s11069-009-9372-5

Marzorati S, Luzi L, De Amicis M (2002) Rock falls induced by earthquakes: a statistical approach. Soil Dyn Earthq Eng 22:565–577

Massey CI, Townsend DT, Lukovic B, Morgenstern R, Jones K, Rosser B, Vilder S (2020) Landslides triggered by the MW7.8 14 November 2016 Kaikōura earthquake: an update. Landslides. https://doi.org/10.1007/s10346-020-01439-x

Nandi A, Shakoor A (2010) A GIS-based landslide susceptibility evaluation using bivariate and multivariate statistical analyses. Eng Geol 110(1–2):11–20. https://doi.org/10.1016/j.enggeo.2009.10.001

Neuhäuser B, Damm B, Terhorst B (2011) GIS-based assessment of landslide susceptibility on the base of the weights-of-evidence model. Landslides. https://doi.org/10.1007/s10346011-0305-5

Newmark NM (1965) Effects of earthquakes on dams and embankments. Geotechnique 15:139–159

Papaioannou Ch, Karakostas Ch, Makra K, Lekidis V, Theodoulidis N, Zacharopoulos S, Margaris V, Rovithis M, Salonikios Th, Morfidis K (2018) The November 17, 2015 MW 6.4 Lefkas, Greece earthquake: Source characteristics, ground motions, ground failures and structural response. In: 16th European conference on Earthquake Engineering, Thessaloniki, 18–21 June 2018

Papathanassiou G, Pavlides S, Ganas A (2005) The 2003 Lefkada earthquake: field observations and preliminary microzonation map based on liquefaction potential index for the town of Lefkada. Eng Geol 82(2005):12–31. https://doi.org/10.1016/j.enggeo.2005.08.006

Papathanassiou G, Valkaniotis S, Ganas A, Pavlides S (2013) GIS-based statistical analysis of the spatial distribution of earthquake-induced landslides in the island of Lefkada, Ionian Islands, Greece. Landslides 10:771–783. https://doi.org/10.1007/s10346-012-0357-1

Papathanassiou G, Valkaniotis S, Ganas A, Grendas N, Kollia E (2017a) The November 17th, 2015 Lefkada (Greece) strike-slip earthquake: Field mapping of generated failures and assessment of macroseismic intensity ESI-07. Eng Geol 220:13–30. https://doi.org/10.1016/j.enggeo.2017.01.019

Papathanassiou G, Valkaniotis S, Ganas A, Pavlides S (2017b) Earthquake-induced landslides in the island of Lefkada, Ionian Islands, Greece, https://doi.org/10.5066/F79G5K96. In: Schmitt R, Tanyas H, Nowicki Jessee MA, Zhu J, Biegel KM, Allstadt KE, Jibson RW, Thompson EM, van Westen CJ, Sato HP, Wald DJ, Godt JW, Gorum T, Xu C, Rathje EM, Knudsen KL (eds) An Open Repository of Earthquake-triggered Ground Failure Inventories. U.S. Geological Survey data release collection. https://doi.org/10.5066/F7H70DB4

Papathanassiou G, Valkaniotis S, Ath G (2021) Spatial patterns, controlling factors and characteristics of landslides triggered by strike-slip faulting earthquakes; case study of Lefkada island, Greece. Bull Eng Geol Environ 80:3747–3765. https://doi.org/10.1007/s10064-021-02181-x

Pavlides S, Papadopoulos GA, Ganas A, Papathanassiou G, Karastathis V, Keramydas D, Fokaefs A (2004) The 14 August 2003 Lefkada (Ionian sea) Earthquake. In: Proc. of the 5th International Symposium on Eastern Mediterranean Geology vol 2, pp 631–635

Pérouse E, Chamot-Rooke N, Rabaute A, Briole P, Jouanne F, Georgiev I, Dimitrov D (2012) Bridging onshore and offshore present-day kinematics of central and eastern Mediterranean: implications for crustal dynamics and mantle flow. Geochem Geophys Geosyst 13:Q09013. https://doi.org/10.1029/2012GC004289

Pradhan B, Youssef A (2010) Manifestation of remote sensing data and GIS on landslide hazard analysis using spatial-based statistical models. Arab J Geosci 3:319–326. https://doi.org/10.1007/s12517-009-0089-2

Rodriguez CE, Bommer JJ, Chandler RJ (1999) Earthquake-induced landslides: 1980–1997. Soil Dyn Earthq Eng 18(5):325–346

Rondoyanni Th, Mettos A, Paschos P, Georgiou Ch (2007) Neotectonic map of Greece, scale 1:100.000, Lefkada sheet. I.G.M.E., Athens

Rondoyanni T, Sakellariou M, Baskoutas J, Christodoulou N (2012) Evaluation of active faulting and earthquake secondary effects in Lefkada Island, Ionian Sea, Greece: an overview. Nat Hazards 61:843–860. https://doi.org/10.1007/s11069-011-0080-6

Rui-Xuan T, Pinnaduwa HSWK, E-Chuan Y, Jing-Sen C (2020) Evaluating landslide susceptibility based on cluster analysis, probabilistic methods, and artificial neural networks. Bull Eng Geol Environ. https://doi.org/10.1007/s10064-019-01684-y

Sachpazi M, Hirn A, Clement C, Haslinger F, Laigle M, Kissling E, Charvis P, Hello W, Lepine J-C, Sapin M, Ansorge J (2000) Western Hellenic subduction and Cephalonia Transform: local earthquakes and plate transport and strain. Tectonophysics 319:301–319

Saroglou H, Asteriou P, Zekkos D, Tsiambaos G, Clark M, Manousakis J (2018) UAV-based mapping, back analysis and trajectory modeling of a coseismic rockfall in Lefkada island, Greece. Nat Hazard 18:321–333. https://doi.org/10.5194/nhess-18-321-2018

Sassa K (2005) Landslide disasters triggered by the 2004 Mid-Niigata Prefecture earthquake in Japan. Landslides 2:135–142. https://doi.org/10.1007/s10346-005-0054-4

Schicker R, Moon V (2012) Comparison of bivariate and multivariate statistical approaches in landslide susceptibility mapping at a regional scale. Geomorphology 161–162:40–57

Schlögel R, Marchesini I, Alvioli M, Reichenbach P, Rossi M, Malet J-P (2017) Optimizing landslide susceptibility zonation: Effects of DEM spatial resolution and slope unit delineation on logistic regression models. Elsevier, 0169–555X, https://doi.org/10.1016/j.geomorph.2017.10.018

Scordilis EM, Karakaisis GF, Karakostas BG, Panagiotopoulos DG, Comninakis PE, Papazachos BC (1985) Evidence for transform faulting in the Ionian Sea: the Cephalonia Island Earthquake Sequence of 1983. Pure Appl Geophys 123:388–397

Sharma LP, Patel N, Ghose MK, Debnath P (2014) Application of frequency ratio and likelihood ratio model for geo-spatial modelling of landslide hazard vulnerability assessment and zonation: a case study from the Sikkim Himalayas in India. Geocarto Int 29:128–146. https://doi.org/10.1080/10106049.2012.748830

Sidle R, Kamai T, Trandafir A (2011) Evaluating landslide damage during the 2004 Chuetsu earthquake, Niigata Japan. Eos 86(13):133–136. https://doi.org/10.1029/2005EO130001

Soeters R, van Westen CJ (1996) Slope Instability Recognition, Analysis and Zonation. In: Turner AK, Schuster RL (eds) Landslides, investigation and mitigation, Transportation Research Board, National Research Council, Special Report 247. National Academy, Washington D.C, pp 129–177

Stringer M, Bastin S, McGann C, Cappellaro C, Kortbawi M, McMahon R, Wotherspoon L, Green R, Aricheta J, Davis R, McGlynn L, Hargraves S, van Ballegooy S, Cubrinovski M, Bradley B, Bellagamba X, Foster K, Lai C, Ashfield D, Baki A, Zekkos A, Lee R, Ntritsos N (2017) Geotechnical aspects of the 2016 Kaikoura Earthquake on the South island of New Zealand. Bulletin of the New Zealand Society for Earthquake Engineering, vol 50, No 2, http://hdl.handle.net/10092/13595.

Tsangaratos P, Loupasakis C, Nikolakopoulos K, Angelitsa V, Ilia I (2018) Developing a landslide susceptibility map based on remote sensing, fuzzy logic and expert knowledge of the Island of Lefkada, Greece. Environ Earth Sci 77:363. https://doi.org/10.1007/s12665-018-7548-6

Underhill JR (1988) Triassic evaporates and Plio-Quaternary diapirism in western Greece. J Geol Soc 145:269–282

van Westen CJ (1997) Statistical landslide hazard analysis. ILWIS 2.1 for windows application guide. ITC Publication, Enschede, pp 73–84

van Westen CJ, Rengers N, Soeters R (2003) Use of geomorphological information in indirect landslide susceptibility assessment. Nat Hazard 30:399–419

Wang HB, Sassa K, Xu WY (2007) Analysis of a spatial distribution of landslides triggered by the 2004 Chuetsu earthquakes of Niigata Prefecture, Japan. Nat Hazard 41:43–60

Wei C, Zenghui S, Jichang H (2019) Landslide susceptibility modeling using integrated ensemble weights of evidence with logistic regression and random forest models. Appl Sci 9:171. https://doi.org/10.3390/app9010171

Xu X, Wen X, Yu G, Chen G, Klinger Y, Hubbard J, Shaw J (2009) Coseismic reverse- and oblique-slip surface faulting generated by the 2008 Mw 7.9 Wenchuan earthquake, China. Geology 37(6):515–518. https://doi.org/10.1130/G25462A.1

Yin Y, Wang F, Sun P (2009) Landslide hazards triggered by the 2008 Wenchuan earthquake, Sichuan, China. Landslides 6:139–151. https://doi.org/10.1007/s10346-009-0148-5

Zekkos D, Manousakis J, Clark M, Cowell K, Medwedeff W, Saroglou H, Tsiambaos G (2017) Satellite and UAV-enabled mapping of landslides caused by the November 17th 2015 Mw 6.5 Lefkada earthquake. In: Proc. of the 19th International Conference on Soil Mechanics and Geotechnical Engineering, pp 2235–2238

Zhao Y, Huang Z, Wei Z, Zheng J, Konagai K (2020) The assessment of earthquake triggered landslides susceptibility with condidering coseismic ground deformation. Nat Hazard. https://doi.org/10.5194/nhess-2020-63